R. & M. No. 3356

MINISTRY OF AVIATION

AERONAUTICAL RESEARCH COUNCIL
REPORTS AND MEMORANDA

A Theoretical Analysis of the Stability of an Aeroplane on Northerly Headings when Controlled by an Aileron-Steering Autopilot Monitored from a Gyro-Magnetic Compass

By H. R. HOPKIN, B.Sc., A.Inst.P., A.F.R.Ae.S.,
M. R. WATTS, G.I.Mech.E. and D. E. FRY

LONDON: HER MAJESTY'S STATIONERY OFFICE
1964
PRICE £1 2s. 6d. NET

A Theoretical Analysis of the Stability of an Aeroplane on Northerly Headings when Controlled by an Aileron-Steering Autopilot Monitored from a Gyro-Magnetic Compass

By H. R. Hopkin, B.Sc., A.Inst.P., A.F.R.Ae.S.,
M. R. Watts, G.I.Mech.E. and D. E. Fry

Communicated by the Deputy Controller Aircraft (Research and Development), Ministry of Aviation

*Reports and Memoranda No. 3356**

May, 1961

Summary.

Long-period lateral oscillations of an aeroplane under automatic control on Northerly headings are shown to be due to high speed in a region of large magnetic-dip angle accompanied by strong monitoring of the gyro-magnetic compass and autopilot. Aerodynamic characteristics are not important, and speed is the predominant aircraft parameter. An approximate analysis assuming that the motion consists of co-ordinated turns is found reliable for many purposes.

The requirement of weak monitoring for ensuring stability conflicts with the need for strong monitoring to restrict datum errors caused by random precession torques on the azimuth gyro and by drifts in the autopilot. Modifications to the compass precession signal may stabilize the motion, but usually at the expense of a deterioration in datum errors, or with insufficient reduction in oscillation amplitude on account of thresholds of rate gyros.

Of the five modifications studied two seem marginally acceptable, but the best way of preventing Northerly-heading oscillations is to employ a good azimuth gyro so that a weak monitor is feasible, or alternatively to monitor the gyro from a sensor that is little affected by aircraft banked turns. The latter requires very good stabilization of the sensor if it is a magnetic detector.

LIST OF CONTENTS

* Replaces R.A.E. Report No. I.A.P. 1467—A.R.C. 23 390.

LIST OF CONTENTS—*continued*

LIST OF APPENDICES

LIST OF ILLUSTRATIONS

---

1. *Introduction.*

It has long been known that a magnetic compass loses accuracy when in a vehicle subjected to rolling disturbances and heading Northwards in the Northern hemisphere. When a pilot tries to fly on a constant Northerly heading using a magnetic compass as a datum, he is very likely to induce an aircraft lateral oscillation. Similar results are obtained with a gyro-magnetic compass but not to such a marked degree.

When (about 1942) the first British 'Distant Reading Compass' was coupled to the Mk. 8 Automatic Pilot in order to provide a heading monitor, undamped oscillations of the order of 2° amplitude with a period of about 2 minutes were observed on Northerly headings. The input signals to the autopilot were however bang-bang, and a reasonable performance was obtained by introducing a dead zone. On the basis of an extremely simplified equation of motion, Sudworth predicted that for this particular type of compass/autopilot system there would always be a critical speed above which instability would obtain on a Northerly heading. The critical speed was inversely proportional to the tangent of the magnetic-dip angle, and could be made higher by reducing the strength of the monitor signal to either the compass or autopilot gyro. The monitors, however, would in practice have to be strong enough to restrain the effects of random torques within prescribed limits.

It was interesting to find some years later (about 1949) that a U.S. Navy aircraft fitted with the Pioneer-Bendix PB10 (A10) autopilot performed in very oscillatory fashion when flying North, even though in this system the magnetic detector was mounted on a vertical gyro.

Instances of long-period oscillations with amplitudes of a few degrees on Northerly headings have been increasing in recent years, presumably owing to higher aircraft speeds in relation to gyro quality. The investigations described in this report were intended to give a fuller understanding of the oscillatory behaviour, and to seek a method of improving a given system without changing any major elements such as gyros.

The initial part of the report introduces approximate equations in anticipation of a justification which appears later. Section 4, which is without reservation labelled *Full Theory*, gives the equations of motion for the aircraft, autopilot and compass, in a form which is thought amply adequate for analysing the dynamics of the complete system when the centre of interest is the susceptibility to oscillate at periods longer than one minute. Stability boundaries based on the full equations are compared with approximate boundaries. Section 5 extends the application of the full equations to analogue-computer response investigations, and some comparison is again made with approximate answers. Section 6 discusses the merits of five proposed modifications to the compass system.

2. *Northerly-Turning Error.*

There does not seem to be a standard definition of Northerly-turning error, and in this report it will be taken as the error introduced into a gyro-magnetic compass when movements of the aircraft (considered as a rigid body) cause the magnetic detector to tilt from the horizontal plane. There are two aspects to be considered. In the first place we are interested in the magnitude of the compass error during and immediately after a turning manoeuvre in which the aircraft heading passes through or approaches North. In the second place we are concerned with what happens when a pilot (human or automatic) tries to fly the aircraft on a constant heading which is not greatly different from North. With idealised linear systems the second aspect would raise the question of whether the aircraft motion is stable or not, or in other words a question of 'Northerly-heading instability' rather than 'Northerly-turning error'. With practical systems, however, we are likely to encounter cases where the motion is stable for large amplitudes but unstable for small ones, and where therefore there will be a residual oscillation whose amplitude and period are important.

The phrase *Northerly*-turning error was evidently coined North of the equator, since exactly equivalent effects are produced in the Southern hemisphere on Southerly headings.

3. *Northerly-Heading Instability.*

3.1. *Basic Cause.*

It is convenient to define the heading of the aeroplane (ψ), the deviation of the azimuth gyro (ψ_c), and the azimuth error of the magnetic detector (ψ_m), relative to magnetic North (*see* Fig. 1). Since the gyro and detector are mounted on the aeroplane, only the relative deviations are in effect available, and it can be shown that the signal obtainable as a measure of the discrepancy between the gyro and the detector is equal to $H \cos \psi \sec (\psi - \psi_m) \sin (\psi_c - \psi_m)$, where H is the horizontal intensity of the earth's magnetic field. Fig. 2 illustrates one way of procuring this signal by compounding two orthogonal signals from the detector with sine and cosine signals from the gyro.

For proportional control the azimuth gyro will be precessed according to the equation

$$\frac{d\psi_c}{dt} = -K_0 H \cos \psi \sec (\psi - \psi_m) \sin (\psi_c - \psi_m),$$

where K_0 is a constant; and if all the angles involved are small, the equation becomes approximately

$$T_c \frac{d\psi_c}{dt} = \psi_m - \psi_c, \tag{1}$$

where the time constant T_c is equal to $1/K_0 H$.

If the magnetic detector is tilted at an angle ϕ_m to the horizontal plane, the explicit relation between ψ_m and ϕ_m is

$$\tan \psi_m = \frac{(1 - \cos \phi_m) \sin \psi \cos \psi + \tan \delta \sin \phi_m \cos \psi}{\cos^2 \psi + \cos \phi_m \sin^2 \psi - \tan \delta \sin \phi_m \sin \psi},$$

where δ represents the angle of magnetic dip. For small tilts this equation becomes approximately

$$\tan \psi_m = \frac{\phi_m \tan \delta \cos \psi}{1 - \phi_m \tan \delta \sin \psi}. \tag{2}$$

At high latitudes ψ_m will be larger because $\tan \delta$ is large, and larger false precession signals will thus be produced, although some alleviation will obtain because the precession rate is also dependent on the value of H.

Admiralty charts (1955) are available which show on a world map, values of vertical, horizontal, North, and East magnetic intensities, also the angle of dip. Two of these are reproduced at the end of this report: Fig. 32 gives the angle of dip, and Fig. 33 gives the horizontal magnetic intensity. Appendix V gives a table of a few extracted values pertaining to the Greenwich meridian.

Thomas[1] has plotted values of ψ_m against ψ for constant values of ϕ_m and δ, using equation (2). When $\phi_m \tan \delta < 1$, ψ_m is zero at $\psi = \pm 90°$, and has turning values at $\psi = \psi_1$ and $180° - \psi_1$, where $\sin \psi_1 = \phi_m \tan \delta$. These turning values are equal to $\pm \psi_1$. On the other hand, when $\phi_m \tan \delta > 1$ there are discontinuities ($\psi_m = \pm 180°$) at $\psi = 90°$, and there are no turning points. These mathematical discontinuities do not represent discontinuities in the real system. When $\phi_m \tan \delta = 1$, the approximate formula is substantially in error near $\psi = 90°$, predicting a discontinuity of $\psi_m = \pm 90°$ at $\psi = 90°$ instead of the correct $\pm 180°$. Green and Glenny[2] have also given curves relating ψ_m and ψ, presumably derived from the accurate formula.

When $\psi = 0$ and ϕ_m is only a few degrees, equation (2) may be further approximated as

$$\psi_m = \phi_m \tan \delta, \tag{3}$$

and (except in Section 6.4.1) this equation has been used in the present investigation, since the autopilot should restrict the aircraft deviations from straight and level flight to sufficiently small values.

The tilt of the detector from the horizontal plane will vary according to the aircraft motion and to the way in which the detector is attached to the aircraft. Thus, if the detector is mounted rigidly to the aircraft the tilt ϕ_m will be the same as the aircraft bank angle ϕ. If the detector is mounted on a vertical gyro, ϕ_m will be equal to the vertical-gyro tilt. If the detector is pendulously mounted—and this is common current practice, as for example in the G4B compass—the tilt ϕ_m will be determined by the direction of the apparent gravity. However, in the latter case, analogue-computer investigations (described in detail later in this report) have shown that because the oscillations produced by Northerly-turning errors have periods that are much longer than those due to 'normal' aircraft aerodynamics, it is usually reasonable to assume that the aircraft is always performing true-banked turns with zero side force. With this assumption the tilt errors of a pendulous detector are the same as those of a rigidly mounted detector, and we can put $\phi_m = \phi$. For small bank angles we can also write

$$g\phi = V \frac{d\psi}{dt},$$

i.e.

$$\phi = T \frac{d\psi}{dt}, \tag{4}$$

where V is the true airspeed, g the acceleration due to gravity, and T a constant having the dimensions of time:

$$T = \frac{V}{g}. \tag{5}$$

For small deviations from a North heading and for small tilts of the detector, equation (1) becomes

$$T_c \frac{d\psi_c}{dt} = T \tan \delta \frac{d\psi}{dt} - \psi_c, \tag{6}$$

and this must be examined in conjunction with another equation defining the changes in aircraft heading ψ imposed by the pilot.

It should be noted that equations (1) and (6) do not include the effect of any torques other than the monitoring torque, so that gyro drift is not included. A steady drift rate d_c would result in a constant error equal to $T_c d_c$. This is important and must be taken into account when assessing the influence of a change in T_c on Northerly-heading instability. However, gyro drift has no effect on the stability of a linear system and is therefore ignored in the analysis that follows.

Pilot's action must depend on the compass indication $(\psi - \psi_c)$, which will be denoted by ψ_i. In order to simplify the analysis, consider an autopilot which causes the aircraft to turn at a rate proportional to the compass signal, so that

$$T_a \frac{d\psi}{dt} = -\psi_i = \psi_c - \psi, \tag{7}$$

where T_a is the compass-monitoring time constant for the autopilot. The aircraft will turn to reduce the heading error from North. It is difficult to deal with the human pilot, but it is reasonable to assume that he acts substantially according to equation (7).

Suppose the aircraft heading is ψ_0 and that the pilot starts to take action. Initially $\psi_c = 0$, so that

$$\frac{d\psi}{dt} = -\frac{\psi_0}{T_a}.$$

At this moment we have from equation (6)

$$\frac{d\psi_c}{dt} = -\frac{T\tan\delta}{T_c}\frac{\psi_0}{T_a},$$

and hence

$$\frac{d\psi_i}{dt} = \frac{\psi_0}{T_a}\left[\frac{T\tan\delta}{T_c} - 1\right].$$

If the quantity in brackets is positive we have the unwelcome consequence that, although the pilot has imposed a turn of the correct sense so as to reduce the heading error, the indicated error ψ_i is increasing. It has been suggested that the condition for stable control is that $T\tan\delta$ must be less than T_c, but this is too stringent. If the time constant T_a is sufficiently great the motion will be stable even if $T\tan\delta > T_c$.

Differentiating equation (7) we have

$$T_c\frac{d\psi_i}{dt} = -T_cT_a\frac{d^2\psi}{dt^2}$$

$$= T_c\frac{d\psi}{dt} - T_c\frac{d\psi_c}{dt}.$$

Using equation (6), we write this as

$$(T_c - T\tan\delta)\frac{d\psi}{dt} + \psi_c,$$

and hence from equation (7) as

$$(T_a + T_c - T\tan\delta)\frac{d\psi}{dt} + \psi,$$

so that finally

$$T_cT_a\frac{d^2\psi}{dt^2} + (T_a + T_c - T\tan\delta)\frac{d\psi}{dt} + \psi = 0. \tag{8}$$

The true condition for stability is that $(T_a + T_c)$ must be greater than $T\tan\delta$. If the damping is small the motion will be oscillatory with a period of $2\pi\sqrt{(T_aT_c)}$ approximately.

If we take $T = 30$ sec (i.e. $V = 30 \times 32{\cdot}2 = 966$ ft/sec or 573 kt) and $\tan\delta = 3$ (i.e. a latitude of about 58°), the motion is stable provided $(T_a + T_c)$ is greater than 90 sec. Typical current values for T_a and T_c would be 25 and 30 sec respectively, which give an unstable condition. For these values the period would be about 55π sec, or just under 3 minutes.

It should be emphasized that the values deduced above are not accurate for autopilots utilising aileron steering as discussed in this report. Nevertheless, the simpler analysis leading to equation (8) does illustrate the basic instability caused by Northerly-turning error and identifies the important parameters.

3.2. *Aileron-Steering Autopilot.*

An aileron-steering autopilot by definition applies aileron as a function of aircraft deviation in yaw as well as in roll. Thus an idealised linear system would produce

$$\xi = F(\phi + c\psi),$$

where ξ is aileron deflection, ϕ is roll deviation, ψ is yaw deviation, and F, c are constants. F is the main gearing or gain, and c is sometimes called the crossfeed ratio.

In practice the aircraft deviations are usually measured by gyros, and, unless these are the basic instruments used by the pilot or navigator, additional monitoring loops must be provided. In this report two varieties of aileron-steering autopilot are considered:

Type 1 employs an aileron equation

$$\dot{\xi} = F\left[\dot{\phi} + c\dot{\psi} + \frac{c}{T_a}(\psi - \psi_c)\right], \tag{9}$$

corresponding to a rate-rate system where the rate of roll $\dot{\phi}$ and rate of yaw $\dot{\psi}$ are measured by rate gyros and the compass signal $(\psi - \psi_c)$ provides the monitoring.

Type 2 has an aileron equation

$$\dot{\xi} = F\left[(\phi - \epsilon) + c(\psi - \psi_c)\right], \tag{10}$$

corresponding to a system making direct use of the compass signal and a signal $(\phi - \epsilon)$ from a bank-angle sensor which is in error by ϵ. In this report we consider a vertical gyro monitored in conventional manner from a pendulum mounted on the roll gimbal or equivalent. For linear erection the precession equation is

$$T_1\dot{\epsilon} = \phi - \epsilon + \alpha_y, \tag{11}$$

where T_1 is the erection time constant, and α_y is the deviation of the pendulum due to the action of aerodynamic side force (*see* Section 4.1). Since at this stage we are assuming that the aircraft is performing true-banked turns, $\alpha_y = 0$, and the gyro tends to precess towards the condition $\epsilon = \phi$, although this is never achieved because the bank angle is continuously changing.

In practice the pendulum monitor may operate in bang-bang fashion according to the equation

$$\dot{\epsilon} = C_\phi \operatorname{sgn}(\phi - \epsilon),$$

where the function sgn(x) has the value $+1$ or -1 according as x is positive or negative. A system incorporating this form of vertical-gyro monitor has not been analysed, but response records were obtained, and these are mentioned later.

Automatic-rudder-control equations are not introduced here: it is merely assumed that the rudder movements are such as to maintain turns co-ordination. Any oscillations whose periods are less than about 10 seconds are ignored, and we can further approximate by putting the right-hand side of equations (9) and (10) equal to zero.

Sections 3.2.1 and 3.2.2 will pursue the approximate analysis relevant to the two types of autopilot and according to the above assumptions. An analysis based on full equations representing aircraft dynamics and complete autopilot will follow in Section 4.

3.2.1. *Approximate stability boundary for Type* 1 *autopilot.*—As already mentioned, in the approximate treatment equation (9) is replaced by

$$\dot{\phi} + c\left[\dot{\psi} + \frac{1}{T_a}(\psi - \psi_c)\right] = 0. \tag{12}$$

This may be compared with the even simpler equation (7), which could have been written

$$\dot{\psi} + \frac{1}{T_a}(\psi - \psi_c) = 0.$$

Combining equations (4), (6) and (12), we obtain a third-order equation instead of second order, and the analysis is simplified if we choose a special unit of time t_1 equal to V/gc, that is T/c. We thus write

$$\overline{T}_c = T_c/t_1,$$
$$\overline{T}_a = T_a/t_1,$$
$$\overline{D} = t_1 D,$$

where $D \equiv d/dt$. Equations (4), (6), (12) then become respectively

$$\phi = c\overline{D}\psi, \tag{4a}$$

$$\overline{T}_c\overline{D}\psi_c = c \tan \delta\, \overline{D}\psi - \psi_c, \tag{6a}$$

$$\overline{D}\phi + c\overline{D}\psi + \frac{c}{\overline{T}_a}(\psi - \psi_c) = 0, \tag{12a}$$

and (4a) and (12a) combine to give

$$\overline{D}^2\psi + \overline{D}\psi + \frac{1}{\overline{T}_a}(\psi - \psi_c) = 0. \tag{13}$$

Eliminating ψ_c from equations (13) and (6a), we obtain the third-order equation

$$J_3\overline{D}^3\psi + J_2\overline{D}^2\psi + J_1\overline{D}\psi + J_0\psi = 0, \tag{14}$$

where

$$J_3 = \overline{T}_a\overline{T}_c,$$
$$J_2 = \overline{T}_a(1 + \overline{T}_c),$$
$$J_1 = \overline{T}_a + \overline{T}_c - c \tan \delta,$$
$$J_0 = 1.$$

According to the Routh-Hurwitz criteria the motion corresponding to equation (14) is stable provided the four coefficients are positive and also $J_2J_1 > J_3J_0$. The latter condition is

$$\overline{T}_a(1 + \overline{T}_c)(\overline{T}_a + \overline{T}_c - c \tan \delta) > \overline{T}_a\overline{T}_c,$$

i.e.

$$\overline{T}_a + \overline{T}_c - c \tan \delta > \frac{\overline{T}_c}{1 + \overline{T}_c}. \tag{15}$$

This form suggests the construction of the diagram in Fig. 3, where the curve represents the function $\overline{T}_c/(1 + \overline{T}_c)$. It should be noted that since T_a, T_c and c are always positive, the condition that the four coefficients be positive is satisfied if (15) is satisfied, and the latter is therefore in practice the sole stability criterion.

In this non-dimensional type of diagram one curve is sufficient to determine whether a system is stable for any combination of the four parameters—aircraft speed V, crossfeed ratio c, and the two time constants T_c, T_a. It is not possible to have a unique scale marked along the boundary curve in order to indicate the period of oscillation P, but in any specific case the period is

$$P = 2\pi\sqrt{\{T_a(t_1 + T_c)\}}. \tag{16}$$

As an example of the use of Fig. 3 consider as before $V = 966$ ft/sec so that $T = 30$. $T_a = T_c = 30$ correspond to $\bar{T}_a = \bar{T}_c = 1$. A typical value for c is unity, and therefore with $\tan\delta = 3$ we locate a point $(1, -1)$ on the diagram. This point is not merely below the stability boundary but below the horizontal axis. For $\bar{T}_c = 1$ stability would be achieved if $\bar{T}_a > 2{\cdot}5$, i.e. $T_a > 2{\cdot}5\ T = 75$ sec. The sum of the monitoring time constants $(T_a + T_c)$ would therefore have to exceed 105 seconds—a more stringent requirement than that obtained in the simple analysis of Section 3.1. In terms of Fig. 3 the simple analysis predicted that the horizontal axis itself would be the stability boundary, but a Type 1 aileron-steering autopilot requires the additional margin represented by the curve $\bar{T}_c/(1+\bar{T}_c)$. Since current practice is to have $\bar{T}_c$ in the range 1 to 2, a rough condition for stability is that

$$c\bar{T}_a + c\bar{T}_c - c\tan\delta > \tfrac{1}{2} \text{ or } \tfrac{3}{4},$$

i.e. (taking the lower figure)

$$T_a + T_c > T\left(\tan\delta + \frac{1}{2c}\right).$$

The effect of varying aircraft speed is represented completely by changes in T, since $T = V/g$.

3.2.2. *Approximate stability boundary for Type 2 autopilot.*—Equation (10) is replaced by

$$\phi - \epsilon + c(\psi - \psi_c) = 0, \tag{17}$$

where

$$T_1\dot{\epsilon} = \phi - \epsilon. \tag{18}$$

Again choosing a special time unit t_1 equal to T/c, we write modified forms of equations (4), (6), and (18):

$$\phi = c\bar{D}\psi, \tag{4a}$$

$$\bar{T}_c\bar{D}\psi_c = c\tan\delta\bar{D}\psi - \psi_c, \tag{6a}$$

$$\bar{T}_1\bar{D}\epsilon = \phi - \epsilon, \tag{18a}$$

where $\bar{T}_c = T_c/t_1$, $\bar{T}_1 = T_1/t_1$, $\bar{D} = t_1 D$. We may eliminate ϕ and ϵ from equations (17), (4a), (18a) to obtain

$$\bar{T}_1\bar{D}^2\psi + (1+\bar{T}_1\bar{D})(\psi - \psi_c) = 0,$$

and eliminate ψ_c from this equation and (6a) to get

$$J_3\bar{D}^3\psi + J_2\bar{D}^2\psi + J_1\bar{D}\psi + J_0\psi = 0, \tag{19}$$

where

$$\begin{aligned} J_3 &= \bar{T}_1\bar{T}_c \\ J_2 &= \bar{T}_1(1+\bar{T}_c) - \bar{T}_1 c\tan\delta, \\ J_1 &= \bar{T}_1 + \bar{T}_c - c\tan\delta, \\ J_0 &= 1. \end{aligned}$$

The motion is stable provided the four J's are positive, and in addition $J_2J_1 > J_3J_0$, i.e.

$$1 + \bar{T}_c - c\tan\delta > \frac{\bar{T}_c}{\bar{T}_c + E}, \tag{20}$$

where

$$E = \bar{T}_1 - c\tan\delta. \tag{21}$$

Stability boundaries based on (20) are shown in Fig. 4, and it is seen that a fixed point (i.e. fixed $\bar{T}_c$ and $c\tan\delta$) can be in a stable region for a particular value of E but in an unstable region if E

becomes less positive as a result of a reduction in $\bar{T}_1$. An increase in the strength of the vertical-gyro pendulum monitor is thus always destabilising. For an unmonitored gyro (i.e. $T_1 = \infty$) the whole of the positive quadrant is the stable region, and the condition for stability is simply $\bar{T}_c > (c \tan \delta - 1)$.

The period of oscillation for any point on the stability boundary is

$$P = 2\pi \left[\frac{T_1 T_c T}{c(T_1 + T_c - T \tan \delta)} \right]^{1/2}. \tag{22}$$

The effect of changing c is not directly indicated by Fig. 4, but it can be shown that an increase in c is stabilizing provided $E < 0$, but destabilizing if $E > 0$. This is clearly seen in Fig. 8 where stability boundaries have been drawn in the T_c, c plane and for particular values of $\tan \delta$, T, T_1. The condition $E = 0$ corresponds to $T_1 = T \tan \delta$, which is 81 seconds in this example.

The boundary for a system with an unmonitored vertical gyro is given by

$$1 + \bar{T}_c - c \tan \delta = 0,$$

and is the horizontal axis in Fig. 4, but a rectangular hyperbola

$$1 + c \left[\frac{T_c}{T} - \tan \delta \right] = 0$$

in Fig. 8.

4. *Full Theory.*

A more accurate representation of the dynamic system consisting of the aeroplane, autopilot, and compass, is obtained by combining the equation of motion of the aeroplane (assumed to be a rigid body), the autopilot control equations (with its servo-systems assumed to have no imperfections), together with the equations for the compass.

4.1. *Aircraft Equations.*

The equations of lateral motion of the aeroplane for small disturbances from straight and level flight are

$$m(\dot{v} + Vr) = mg\phi + \Delta Y, \tag{23}$$

$$A\dot{p} = \Delta L, \tag{24}$$

$$C\dot{r} = \Delta N, \tag{25}$$

where m is the aircraft mass, v is the increment of velocity along the y axis (i.e. the sideslip velocity), V is the steady datum speed of the aeroplane in undisturbed flight, r is the angular velocity $\dot{\psi}$ about the z axis (yaw), g is the acceleration due to gravity, ϕ is the bank-angle disturbance, ΔY is the increment of aerodynamic force along the y axis, A and C are the aircraft moments of inertia about the x and z axes respectively, p is the angular velocity $\dot{\phi}$ about the x axis (roll), ΔL and ΔN are the increments of aerodynamic rolling and yawing moments. Products of inertia have been neglected. For small increments v, ϕ, p, r, etc. it is usual to expand ΔY, ΔL, ΔN, in terms of derivatives:

$$\Delta Y = \Sigma \frac{\partial Y}{\partial v} v = Y_v v + \ldots,$$

$$\Delta L = L_v v + \ldots,$$

$$\Delta N = N_v v + \ldots,$$

where Y_v is written for $\partial Y/\partial v$, and so on.

The derivatives are constants for a particular aeroplane at a particular flight condition and are quoted in non-dimensional form as outlined in Appendix I. Including only the derivatives that are usually significant we write

$$\Delta Y = Y_v v + Y_\zeta \zeta, \tag{26}$$

$$\Delta L = L_v v + L_p p + L_r r + L_\xi \xi, \tag{27}$$

$$\Delta N = N_v v + N_p p + N_r r + N_\xi \xi + N_\zeta \zeta, \tag{28}$$

where ξ and ζ are the increments of aileron and rudder displacements.

It should be noted that a pendulous element whose pivots are fixed parallel to the x axis of the aeroplane (i.e. a transverse pendulum) will hang at an angle $(\phi + \alpha_y)$ to the vertical, where α_y is the angle between the pendulum and the aeroplane's longitudinal plane of symmetry, and is given approximately by

$$\alpha_y = \frac{\Delta Y}{mg}, \tag{29}$$

if the natural frequency of the pendulum is high compared with the frequency of the measured quantity.

4.2. *Autopilot Equations.*

It is convenient to consider first the aileron equations for both the Type 1 and Type 2 autopilots, and then the corresponding rudder equations.

Aileron equations.—Type 1 autopilot has been assumed to have a rate-rate servo-system with input signals provided by roll and yaw rate gyros. It should not be assumed that these signals are perfect, and instead of equation (9) we should write

$$\dot{\xi} = F\left[p_a + cr_a + \frac{c}{T_a}(\psi - \psi_c)\right], \tag{30}$$

where p_a and r_a represent real gyro signals. We are not concerned in this investigation with relatively high-frequency phenomena, so there is little point in including the dynamic characteristics of either the rate gyros or the servo-system, but we have examined the effects of thresholds in the gyro signals.

Type 2 autopilot makes use of position gyros, and beyond taking account of their monitoring systems—which has been done in equation (10)—there seems no need to investigate any further practical complications. Dynamic effects of gimbal-ring inertia are significant only at high frequency, and random wander has no influence on stability, although it does cause steady-state errors and in this respect is roughly equivalent to rate-gyro threshold.

Rudder equations.—When heading is controlled by the aileron channel of an autopilot the function of the rudder channel is to ensure adequate damping of the 'yaw' short-period oscillation and also to suppress aerodynamic side force ΔY. To this end the basic rudder equation is usually

$$\zeta = H_1 r + H_2 f(\alpha_y), \tag{31}$$

but the precise form depends on the design of the servo-system and whether an autostabilizer mode has to be provided. Sometimes the rudder action will be made a function of rate of roll and of aileron movement in addition to the terms of equation (31) in order to improve control co-ordination during transitions between straight and turning flight, but such a rudder equation has not been used in this investigation.

In a Type 1 autopilot a rate-rate version of equation (31) would be used, and a signal representing $\dot{r}$ would be obtained either from an angular accelerometer or by differentiating a rate-gyro signal. In the latter case a passive network might be employed, and the rudder equation would probably be

$$\dot{\zeta} = \frac{H_1 D}{1 + \tau_1 D} r_a + H_2 \alpha_y, \tag{32}$$

where the network time constant τ_1 is small compared with the yaw oscillation period.

In a Type 2 autopilot whose rudder channel must also operate in an autostabilizer mode, the equation might be

$$\zeta = \frac{H_1 \tau_1 D}{1 + \tau_1 D} r_a + H_2 \int \alpha_y dt, \tag{33}$$

where τ_1 is the time constant of a filter or 'washout' network designed to minimise opposition to pilot control during manoeuvres.

It is reasonable to assume that the passive networks just mentioned have negligible influence on the long-period motions resulting from tilt errors of the compass magnetic detector. The same rudder equation has therefore been used in this investigation for both Type 1 and Type 2 autopilots, and has the form

$$\dot{\zeta} = H_1 \dot{r}_a + H_2 \alpha_y. \tag{34}$$

4.3. *Compass Equations.*

The azimuth-gyro precession equation (1) is always valid when the pick-off, amplifiers, and torque motor are operating inside their linear range, but equation (3) must be applied with $\phi_m = \phi + \alpha_y$ in order to allow for the transverse pendulosity of the magnetic detector, and the simpler equation (6) should not be used. Remembering also that equation (4) is replaced by equation (14), which may be written as

$$\phi + \alpha_y = T\dot{\psi} + \frac{\dot{v}}{g}, \tag{14a}$$

we derive the replacement for equation (6):

$$T_c \dot{\psi}_c = \tan \delta \left(T\dot{\psi} + \frac{\dot{v}}{g} \right) - \psi_c. \tag{35}$$

By combining this equation with the autopilot equations (34), (30) or (10), and with the aircraft equations (23), (24), (25), we can examine the dynamic behaviour of the complete system.

In a real system the linear equation (35) will not apply when it demands a larger precession rate than is possible in the equipment, and in the response investigations of Sections 5 and 6 we have assumed that the precession rate stays at the maximum value in these circumstances.

It may be convenient to use a normalised form of the equations, which corresponds to the non-dimensional form of the aerodynamic data, and details are given in Appendices I and II, while the numerical data employed in this investigation are given in Appendix III.

4.4. *Stability Boundary.*

It has already been shown that approximate equations result in fairly simple stability criteria which were illustrated in Figs. 3 and 4. The analysis is much more tedious for the fuller equations

described in Sections 4.1, 4.2, 4.3, but it is reasonably accurate to seek neutral stability conditions by means of an analogue computer. The ringed points marked in Figs. 5 and 8 correspond to neutral stability for a Type 1 autopilot in aeroplane A and for a Type 2 autopilot in aeroplane B respectively, while the full lines give the neutral stability conditions predicted by the approximate equations. For the purpose of this stability work only, the full equations (34) and (30) have been assumed to have rate-gyro terms with zero thresholds and (35) to have no limitation on available precession rate.

Fig. 5 refers to $\tan \delta = 3$, $c = 1$, and $T = 27$. The approximate theory demands that in order that the system should be stable $(T_a + T_c)$ should be greater than the value of $t_1 c \tan \delta + t_1 T_c/(t_1 + T_c)$, in this case $81 + 27 T_c/(27 + T_c)$ and varying from 81 sec to 108 sec as T_c increases from zero to infinity. It is seen that according to the full equations neutral stability is obtained along a curve roughly parallel to the approximate stability boundary and below it by about 3 or 4 seconds. This corresponds to a discrepancy of about 5% in $(T_a + T_c)$. The degree of precision achievable on the analogue computer may be assessed from Fig. 6, which shows the actual records obtained for T_c, T_a values corresponding to the points X, Y, Z on Fig. 5. The first record is damped, the second very slightly divergent and the third decidedly divergent. The periods of oscillation measured from analogue-computer records are 325 sec, 370 sec, 269 sec, whereas the approximate equation (16) predicts 331 sec, 379 sec, 276 sec respectively, which are in good agreement.

Since the approximate theory is adequate for most purposes for predicting the inherent stability of the system, diagrams showing directly the effects of variations in speed or some other parameter may be derived from the stability criterion (15). Fig. 7 for instance gives the stability boundaries for each of the values $V/c = 700$, 800, 900, 1,000 ft/sec when $\tan \delta = 3$.

Turning now to the Type 2 autopilot and Fig. 8 we again find good agreement between full and approximate equations. The values $\tan \delta = 3$ and $T = 27$ have been used once more, together with the three values $T_1 = 33$, 66, 81 sec and also $T_1 = \infty$ which represents an unmonitored vertical gyro. The largest discrepancy in the value of T_c to give zero damping is only 5 sec. The periods of oscillation are also given reasonably well by the approximate formula (22), as marked along the curves.

Fig. 9 gives the approximate-theory stability boundaries for each of the speeds $V = 800$, 1000, 1200, 1400 ft/sec when $\tan \delta = 3$ and $T_1 = 33$ sec.

5. *Response Investigation Including Non-Linearities.*

In this investigation we have examined the significance of limiting the azimuth-gyro precession rate, of rate-gyro thresholds in a Type 1 autopilot, and of bang-bang erection of the vertical gyro in a Type 2 autopilot. It is considered unnecessary to include limiting of the rate-gyro signals since the gyros are designed to cope with aircraft short-period response where the angular velocities are very much higher than those occurring in the long-period Northerly-heading oscillations.

5.1. *Limiting of Azimuth-Gyro Precession Rate.*

The amplifier and torque motor for precessing the azimuth gyro are often designed to have maximum outputs two or three times as much as should be required for preventing the worst expected gyro wander rate. The safety factor depends on the consistency of gyro behaviour and on whether steps are taken to compute and allow for errors due to the earth's rotation and to the curved path of the aeroplane around the earth. The actual limiting value also depends on the intrinsic quality of the gyro.

For a gyro designed to have a wander rate up to 1/4 deg/min, but whose in-service apparent drift may be 1/2 deg/min, or even 1 deg/min, owing to deterioration and to the omission of computed corrections, the limiting precession rate is likely to be two or three degrees per minute. In this investigation a value of 2·5 deg/min has been used in most cases.

It would be expected that limiting of the precession rate should convert the divergent oscillatory response of a basically unstable system into a steady oscillation whose amplitude is determined by the saturation level. Figs. 10, 11, 12 illustrate this effect. Some records were obtained by applying the full equations, and others from the approximate equations of Section 3.2 with limiting introduced. The agreement between the full and approximate theory is very good in all cases.

It would be useful if the amplitude of oscillation could be predicted. Examination of the records in Fig. 10 reveals that the yaw amplitudes are approximately halved each time the limiting precession rate is halved, whereas the period is almost unaltered at about 316 sec. If we assumed the waveform to be triangular we would calculate the amplitudes to be 3·3°, 1·65°, 0·825° for precession rates of 2·5 deg/min, 1·25 deg/min, 0·625 deg/min respectively. These are not seriously different from the record values of 3·16°, 1·67°, 0·925° respectively. However, in order to do this calculation we must know the period. A rough estimate might be obtained from the approximate equations (14) or (19), or even from equations (16) or (22) if the system when linear is not far from the neutral stability condition.

The factors of the stability cubic

$$\lambda^3 + L_2\lambda^2 + L_1\lambda + L_0,$$

obtained from the differential equation (14) by putting $L_i = J_i/J_3$, may usually be obtained to any degree of accuracy by the following iterative process. Guess a_i and then calculate $c_i = L_0/a_i$, $d_i = c_i/a_i$, $b_i = (L_1 - c_i)/a_i$, $e_i = L_2 - b_i - a_i$, $T_i = 1 + (d_i - b_i)/a_i$, from which the next guess $a_{i+1} = a_i + e_i/T_i$ is obtained. The factors of the cubic will after some iteration be represented approximately by $(\lambda + a_i)(\lambda^2 + b_i\lambda + c_i)$, as the test quantity e_i tends to zero. The first value a_1 is taken as $a_1 = L_2 - b_0$, where $c_0 = L_0/L_2$, $b_0 = (L_1 - c_0)/L_2$.

As an example, consider the system whose behaviour is shown in Fig. 10. We use equation (14) and parameter values $T = 27$, $c = 1$, $\tan\delta = 3$, $T_a = 25$, $T_c = 30$, so that $\bar{T}_a = 0{\cdot}9259$, $\bar{T}_c = 1{\cdot}1111$. The stability cubic is

$$\lambda^3 + 1{\cdot}9\lambda^2 - 0{\cdot}9362\lambda + 0{\cdot}972,$$

and the coefficient of λ^2 is equal to $(1 + 1/\bar{T}_c)$ that is $(1 + T/cT_c)$. We calculate $c_0 = 0{\cdot}5116$, $b_0 = -0{\cdot}7620$ to get $a_1 = 2{\cdot}6620$. The first iteration then yields $c_1 = 0{\cdot}3651$, $d_1 = 0{\cdot}1372$, $b_1 = -0{\cdot}4888$, $e_1 = -0{\cdot}2732$, $T_1 = 1{\cdot}2352$, and hence $a_2 = 2{\cdot}4408$. The second iteration gives $c_2 = 0{\cdot}3982$, $d_2 = 0{\cdot}1631$, $b_2 = -0{\cdot}5467$, $e_2 = 0{\cdot}0059$, $T_2 = 1{\cdot}2908$, and the next trial value would be $a_3 = 2{\cdot}4454$.

The factors $(\lambda + a_1)(\lambda^2 + b_1\lambda + c_1)$ will often be good approximations, and in the example the quadratic factor $(\lambda^2 + b_1\lambda + c_1)$ is $(\lambda^2 - 0{\cdot}4888\lambda + 0{\cdot}3651) = (\lambda - 0{\cdot}2444 \pm 0{\cdot}5526i)$, which corresponds to a period of $2\pi/0{\cdot}5526$ expressed in units of $t_1 = 27$ sec, that is a period of 307 sec. This agrees well with the analogue-computer result of 316 sec. The formula (16) however gives 237 sec, which is a poor estimate because the system is nowhere near the neutral stability condition. Applying the first routine to the cases of Fig. 11 we obtain approximate factors $(\lambda + 2{\cdot}02)(\lambda^2 - 0{\cdot}29\lambda + 0{\cdot}321)$, $(\lambda + 1{\cdot}63)(\lambda^2 - 0{\cdot}138\lambda + 0{\cdot}298)$, $(\lambda + 2{\cdot}04)(\lambda^2 - 0{\cdot}125\lambda + 0{\cdot}238)$ for the second, third, and fourth cases respectively and the periods calculated from these factors are 310, 313, 351 sec. Triangular

waveforms at these periods would have amplitudes of 3·2°, 3·3°, 3·6° respectively. The periods measured from the records are 316, 315 and 368 sec respectively, and the measured amplitudes are 3·1°, 2·85°, 3·1°.

The iterative chain will not converge unless the coefficient L_2 is sufficiently pivotal[3]. Thus, if $c \tan \delta$ is large L_1 is more likely to be pivotal, and then the approximate factors would be $(\lambda^2+L_2\lambda+L_1)\ (\lambda+L_0/L_1)$. For example, if $c \tan \delta$ is 12 and $\overline{T}_a = 0{\cdot}9259$, $\overline{T}_c = 1{\cdot}1111$ as above, the cubic is

$$\lambda^3 + 1{\cdot}9\lambda^2 - 9{\cdot}6841\lambda + 0{\cdot}972,$$

and has factors $(\lambda^2+2{\cdot}0025\lambda-9{\cdot}4787)\ (\lambda-0{\cdot}1025)$, or $(\lambda-2{\cdot}2362)\ (\lambda+4{\cdot}2388)\ (\lambda-0{\cdot}1025)$. In this case the linear system has an inherent divergent exponential mode, rather than a divergent oscillation, and the period of a limit cycle is not directly predictable.

Passing to the Type 2 autopilot and Fig. 12, we again find that halving the limiting precession roughly halves the amplitude without altering the period. Thus for $c = 1$, $T_1 = 33$, amplitudes of 3·8° and 1·98° are obtained at a period of 290 sec; and for $c = 1$, $T_1 = \infty$, the amplitudes are 2·3°, 1·2° and the period is 273 sec. Amplitudes calculated for triangular waveforms and these periods would be 3·0° and 1·5°, and 2·8°, 1·4° respectively. These values are about 20% in error.

It is easier to consider $T_1 = \infty$ because the stability cubic corresponding to equation (19) degenerates into a quadratic

$$\lambda^2 + L_1\lambda + L_0,$$

where

$$L_1 = \frac{1 + \overline{T}_c - c \tan \delta}{\overline{T}_c},$$

$$L_0 = \frac{1}{\overline{T}_c}.$$

Substituting the values for Fig. 12 ($c = 1$) we have $\overline{T}_c = 25/27 = 0{\cdot}9259$, $c \tan \delta = 3$, and hence $L_1 = -1{\cdot}074$, $L_0 = 1{\cdot}08$. The quadratic has factors $(\lambda-0{\cdot}537\pm0{\cdot}8898i)$, corresponding to a divergent oscillation of period 191 sec, as compared with the limit-cycle period of 273 sec. This approximation is therefore not a good basis for predicting either the period or amplitude of the limit cycle. As for the Type 1 autopilot, a large value of $c \tan \delta$ would result in the linear system having a divergent exponential mode.

We may summarise the results obtained in this section as follows:

For the range of values considered for the Type 1 autopilot the period is always about 5 min and the amplitude of oscillation is determined almost completely by the value of the limiting precession rate of the compass gyro. For the Type 2 autopilot the amplitude is proportional to the limiting precession rate but is also sensitive to changes in the time constant T_1 of the vertical-gyro pendulum monitor. A reduction in T_1 makes the amplitude greater. The typical period for a Type 2 autopilot seems to be about 4 to 4½ min.

5.2. *Thresholds of Autopilot Rate Gyros.*

Fig. 13 shows the effect on aircraft response of thresholds in the roll and yaw rate gyros of a Type 1 autopilot. The records are for East/West flight and were obtained by putting $\tan \delta = 0$. It is seen that a yaw-gyro threshold induces a residual oscillation whose amplitude and frequency are modified by changes in roll-gyro threshold. An increase in the latter reduces the amplitude and

increases the frequency. For equal thresholds of 1 deg/min on the two gyros the residual oscillation has an amplitude of 0·25° and a period of 80 sec and for thresholds of 2 deg/min these quantities become 0·55° and 90 sec.

Fig. 14 shows that when tan δ is gradually changed from zero to 3 (which may be interpreted as changing the heading from East/West to North), there is a continuous transition both in amplitude and period from 0·25° and 80 sec to 3·3° and 320 sec when the gyro thresholds are ± 1 deg/min. It is remarkable that when tan $\delta = 3$ the 3·3° amplitude oscillation caused by the magnetic-detector tilt errors is completely predominant and there is no trace of any superimposed oscillation having a period of 80 sec. When tan $\delta = 2$ the gyro thresholds reduce the amplitude slightly, but below tan $\delta \approx 1{\cdot}51$ the linear system is stable and the thresholds cause a residual oscillation which would not otherwise be there.

5.3. *Bang-Bang Erection of Vertical Gyro.*

A vertical gyro is often monitored from a simple mercury switch, and the precession equation is then

$$\dot{\epsilon} = C_\phi \operatorname{sgn}(\phi - \epsilon),$$

as mentioned in Section 3.2, unless there is also a dead space so that $\dot{\epsilon} = 0$ when $|\phi - \epsilon|$ is less than a prescribed amount. A typical value for the constant precession rate is $C_\phi = 2{\cdot}5$ deg/min, and a dead space of about $\pm 1/8°$ is likely.

Response records were taken for these values, but the effect of a dead space of this magnitude was found to be negligible, and therefore only records of systems with pure bang-bang erection are shown (Figs. 15 and 16).

The first diagram shows that as tan δ is reduced there is a change from a limit cycle to a damped motion whether the vertical gyro is unmonitored or bang-bang monitored, but in the latter case a limit cycle is present down to a lower value of tan δ. Compare, for instance, the records for tan $\delta = 1$.

All the records in Fig. 15 are for a crossfeed ratio of 2, and Fig. 16 gives results for $c = 4$ and $c = 1$ when tan δ is zero or three. Comparing the records for tan $\delta = 3$, $c = 1, 2, 4$ in Figs. 15 and 16, and also $c = 4$, $T_1 = 33, \infty$ in Fig. 12, we see that the amplitude and period of the limit cycle are not much affected by the changes in parameters or even the changes from bang-bang to linear to no erection. This is presumably because the system is well and truly unstable. When, however, tan δ is reduced and the system with unmonitored vertical gyro is only just stable or unstable, the effects of parameter changes become noticeable. Similarly, when we compare linear erection with $T_1 = 33$ and no erection ($T_1 = \infty$) for $c = 1$, we can see in Fig. 8 that the behaviour of a system with $T_c = 30$ is much more sensitive to changes in T_1 than the corresponding system with $c = 4$. The appreciable difference between the third and fourth rows in Fig. 12 is therefore not surprising.

6. *Stabilizing Schemes.*

A study was made of the possibility of improving the behaviour of the system by simple modification. It is clear that the most direct and fundamental cure is either to design an azimuth gyro which requires only a low monitor strength, or to eliminate the tilt error of the monitor datum. However, this investigation was started on the assumption that equipment of a certain calibre already existed, and hence there was a severe limitation to the kinds of modification that could be proposed.

In all the schemes discussed below there is liable to be a deterioration in accuracy owing to the effect of the modification on the azimuth-gyro monitor when the latter is opposing random precession torques. There is then a conflict between this factor and the degree of improvement to the stability or amplitude of the unwanted oscillation.

Examination of the stabilizing schemes has been mainly done in relation to a Type 1 autopilot, because there is little difference essentially between the results obtained with the two autopilots, and because the Type 1 has the added complication of rate-gyro thresholds.

6.1. *Dead Zone.*

Sometimes it is possible to reduce the amplitude of a limit-cycle oscillation by introducing a dead zone on one of the signals. In the autopilot/compass system the reasonable place to introduce a dead zone seems to be where the compass signal is fed into the autopilot. This would reduce the accuracy of the autopilot datum heading but would not impair the compass heading information fed to navigation systems.

Response records showed that although some improvement is possible the stability of the system becomes very dependent on the size of any disturbance. Following a disturbance larger than a certain value the motion is oscillatory and rapidly divergent. Since the critical value of disturbance was small (e.g. $0{\cdot}5°$ in yaw), the dead-zone modification was not considered further.

6.2. *Augmented Feedback.*

It was proposed that the azimuth-gyro precession signal be supplemented by an amount proportional to the compass output signal $(\psi - \psi_c)$. The precession equation (1) is then replaced by

$$T_c \frac{d\psi_c}{dt} = \psi_m - \psi_c + K_1(\psi - \psi_c), \tag{36}$$

and the approximate equation of motion for a Type 1 autopilot is

$$J_3\bar{D}^3\psi + J_2\bar{D}^2\psi + J_1\bar{D}\psi + J_0\psi = 0, \tag{37}$$

where

$$\begin{aligned} J_3 &= \bar{T}_a\bar{T}_c, \\ J_2 &= \bar{T}_a(1+\bar{T}_c+K_1), \\ J_1 &= \bar{T}_a + \bar{T}_c - c\tan\delta + K_1\bar{T}_a, \\ J_0 &= 1. \end{aligned}$$

The destabilizing negative term in J_1 can therefore be annulled by having $K_1 = c\tan\delta/\bar{T}_a = T\tan\delta/T_a$, but a lower value is sufficient to make the motion stable. For example, when $T = T_a = T_c = 30$, $c = 1$, and $\tan\delta = 3$, exact cancellation is obtained with $K_1 = 3$, and the motion is neutrally stable with $K_1 = 1{\cdot}3$.

Steady-state errors due to constant drift in the autopilot and compass systems may be determined from the relations

$$\begin{aligned} T_a d_a &= c(\psi - \psi_c) \\ T_c d_c &= \psi_c - K_1(\psi - \psi_c), \end{aligned}$$

where d_a and d_c represent the drift in the autopilot and compass respectively. The autopilot must fly the aeroplane off course by an amount

$$\psi - \psi_c = T_a d_a/c \tag{38}$$

in order to maintain a steady state with $\dot{\xi} = p = r = 0$, and the azimuth gyro must stay off datum by an amount

$$\psi_c = T_c d_c + K_1 T_a d_a / c$$

in order to maintain zero precession rate $\dot{\psi}_c$. For $T_c = T_a = 30$ and $c = 1$ the compass error is $30(d_c + K_1 d_a)$. We have already established that K_1 is of the order of 2 or 3 in order to produce stability, and if we further assume that the autopilot drift level is liable to be several times higher than the compass drift, we see that the compass error may well be ten times as large as the design value. The autopilot error (38) is often unimportant since the aircraft heading can be corrected by the pilot through the autopilot turn inceptor[4].

Response records were taken (*see* Fig. 17) to examine whether a low value of K_1 might produce a useful reduction of limit-cycle amplitude, and also to see the effect of autopilot gyro threshold. When $K_1 = 1$ the amplitude is about $2 \cdot 7°$ whether there are thresholds or not, and with thresholds present even the 'stable' values $K_1 = 2$ and 3 give amplitudes of $2°$ and $1 \cdot 5°$ respectively.

The results indicate that it is not possible to find a value of K_1 which would be acceptable both for good response and small datum errors in the presence of drift.

6.3. *Rate-Gyro Feedback.*

Since an approximate theory assuming co-ordinated turns seems reliable, and the false signal from the magnetic detector is thereby proportional to bank angle or rate of turn, it was suggested by R.A.E. that an opposing signal from a yaw rate gyro would stabilize the system provided the quality of the signal were good enough. The compass precession equation would be

$$T_c \dot{\psi}_c = \psi_m - \psi_c - K_b T r_b, \tag{39}$$

where r_b represents the signal supplied by a rate gyro which is not necessarily the same as the autopilot yaw rate gyro.

Since $\psi_m = rT \tan \delta$ approximately, the value of K_b corresponding to exact cancellation would be $\tan \delta$. The coefficients of the stability cubic for a Type 1 autopilot are

$$J_3 = \bar{T}_a \bar{T}_c,$$
$$J_2 = \bar{T}_a(1 + \bar{T}_c),$$
$$J_1 = \bar{T}_a + \bar{T}_c + c(K_b - \tan \delta),$$
$$J_0 = 1,$$

if it is assumed for the moment that $r_b = r$. Neutral stability is obtained with

$$K_b = \tan \delta - \frac{1}{c}\left[\frac{\bar{T}_c^2}{1 + \bar{T}_c} + \bar{T}_a\right],$$

which, for example, has a value of $1 \cdot 5$ when $T_a = T_c = T$, $\tan \delta = 3$, $c = 1$.

Steady-state errors due to drifts d_c and d_a in compass and autopilot respectively, and to a threshold d_b in the extra stabilizing rate gyro, are determined by the relations

$$T_a d_a = c(\psi - \psi_c),$$
$$T_c d_c = \psi_c - K_b T d_b.$$

The compass error is thus $(T_c d_c + K_b T d_b)$.

It seems reasonable to assume that since the r_b signal is merely required for stabilizing a long-period oscillation, the rate gyro need not cope with large rates of yaw and could be designed to have a fairly low threshold. If the value of d_c includes the apparent drift due to earth's rotation and to curved flight path it is practicable to design a rate gyro with d_b smaller than d_c. If $d_b = d_c/3$, $T_c = T$, and $K_b = 3$, the compass error is then double the design value. The deterioration in steady-state error caused by the rate-gyro stabilizing scheme seemed moderate enough to justify a theoretical investigation into the dynamic behaviour when rate-gyro thresholds and limiting of the compass-gyro precession were included.

A very limited and inconclusive flight investigation was also made in which the stabilizing rate gyro was an improvised modification of a standard autopilot rate gyro. The sensitivity was increased appreciably and the maximum measurable rate correspondingly reduced; laboratory tests indicated an extremely low threshold, but the value in flight is not known. Flight records showed that one of the disadvantages of feeding a yaw rate-gyro signal into the compass-precession amplifier is that the aircraft yaw oscillation produces enough 'noise' to cause the amplifier output to saturate positively and negatively in almost bang-bang fashion. It seemed possible that there was still enough rate-gyro influence at long periods to improve the compass oscillation as intended, but there was insufficient evidence and further flight tests could not be made. Filtering of the rate-gyro signal is an obvious possibility, and the efficiency of a one-stage filter was examined during the theoretical investigation.

Fig. 18 illustrates the aircraft response in yaw (ψ), and also the compass-precession rate ($\dot{\psi}_c$), for $K_b = 2{\cdot}2, 3{\cdot}3, 5{\cdot}5$ with and without rate-gyro thresholds included. The threshold on the stabilizing gyro was taken as $\pm 0{\cdot}25$ deg/min—a quarter of the autopilot gyro thresholds. The influence of thresholds is quite marked when $K_b = 2{\cdot}2$, forcing an amplitude of $1{\cdot}13°$. When $K_b = 3{\cdot}3$ the amplitude is $0{\cdot}43°$ and $K_b = 5{\cdot}5$ produces an amplitude of $0{\cdot}21°$ which is practically identical with the best performance available from autopilot gyros with ± 1 deg/min thresholds even when there is no Northerly-heading compass error (*see* last record of first column in Fig. 14).

Fig. 19 shows the effect of a filter with transfer function $1/(1+\tau D)$ when the time constant τ is varied, and K_b kept constant at $3{\cdot}3$. There is a continuous degradation in performance of the stabilizing signal, and the amplitude in yaw increases from $0{\cdot}4°$ at $\tau = 0$ no (i.e. filter) to $1{\cdot}43°$ at $\tau = 10$ sec. Fig. 20 shows the corresponding short-period transient response to an arbitrary triangular side-gust pulse of duration $0{\cdot}6$ sec. It would appear that a time constant of at least 5 sec is required in order to reduce substantially the number of times that the compass precession rate reaches its limiting value. It was not thought worthwhile to simulate typical gusty weather, since there is little doubt over the order of magnitude of filter time constant required. The amplitudes in Fig. 19 are $1{\cdot}43°$, $0{\cdot}74°$, $0{\cdot}5°$ for $\tau = 10, 5, 2{\cdot}5$ sec respectively.

Fig. 21 compares (on a different scale) the results for $T_c = 30$ sec with the corresponding ones for $T_c = 60$ sec. The amplitudes in degrees for $\tau = 10, 5, 2{\cdot}5$ and 0 sec are as follows:

	Filter time constant, τ			
	10	5	2·5	0
$T_c = 30$	1·59	0·74	0·54	0·37
$T_c = 60$	0·9	0·4	0·28	0·19

The values obtained for $T_c = 30$ should agree with those quoted for Fig. 19. The small discrepancies arose because the records were obtained on different occasions on different computers, and it is difficult to set the non-linear units to exactly the same characteristics. This is relevant in this particular investigation, for the amplitude is determined by the non-linearities.

The benefit to be obtained from a rate-gyro stabilizing signal thus depends very much on the precise magnitudes of the thresholds of all the rate gyros and on the combination of K_b and filter time constant that can be used.

6.4. *Amplifier Modifications.*

It was suggested by A. & A.E.E. that a simple circuit modification within the precession amplifier would improve the dynamic performance. The modification may be loosely called an integrator and theoretically the result is to introduce an additional factor $1/(1+\tau_3 D)$ in the transfer function of the amplifier, at least within the linear range. The proposed value of the time constant τ_3 was about 50 sec.

The analysis of Appendix IV shows that an unstable system with $T_a + T_c < T \tan \delta$ cannot be made stable by any choice of τ_3, and that the modification will impose stability on an unstable system with $T_a + T_c > T \tan \delta$ only if $T_c < T \tan \delta$. The chance of being able to obtain a basically stable system is therefore small. However, it is difficult to predict the limit-cycle amplitudes of non-linear systems, and therefore analogue-computer results were obtained. Fig. 22 shows that the limit-cycle amplitude for typical parameter values is increased and the period lengthened.

The Sperry Gyroscope Co. proposed a somewhat similar scheme, introducing a factor $(1+\tau_2 D)/(1+\tau_3 D)$ in the amplifier transfer function. The values of τ_2 and τ_3 were 150 sec and 300 sec respectively and were to be used in conjunction with $T_c = 60$ sec.

Appendix IV shows that various combinations of τ_2 and τ_3 values can stabilize a linear system. The general shape of the stability boundary is illustrated in Fig. 23, and specific examples given in Fig. 24 for three combinations of time constants:

	(a)	(b)	(c)
T_c(sec)	30	30	60
T_a(sec)	25	50	25

Fig. 25 gives response records obtained for (a), and (c) with and without autopilot gyro thresholds taken into account. For (a), values of τ_2 and τ_3 represented by the point Q in Fig. 24 were taken in order to have a basically stable system. Gyro thresholds as usual produce a residual oscillation, and its amplitude is 0·19°. The representative point P was also considered because Sperry had suggested $\tau_2 = 150$, $\tau_3 = 300$. It is seen that with these values it is essential to have T_c larger than 30 sec in order to make the amplitude small.

Fig. 26 illustrates the performance of various other combinations of τ_2 and τ_3 in conjunction with combinations (a), (b), or (c). The first two pairs of records refer to the point R in Fig. 24, which indicates that time constants (a) should produce an unstable linear system, and (b) a stable one. The records bear this out. Rate-gyro thresholds of ± 1 deg/min, as noticed earlier, exert little influence on the large amplitude of a basically unstable system. In case (b), however, the linear system is only just stable and gyro thresholds tip the balance so that the amplitude grows to a steady value (not shown).

The third and fourth pair of records refer to the point S in Fig. 24, so that time constants (b) would be expected to give an unstable linear system, and (c) a stable one. This again is confirmed by the records, and the contrast between the steady amplitudes and periods in the presence of rate-gyro thresholds is pronounced: 3·1° at a period of 369 sec and 0·26° at a period of 105 sec.

The final pair of records refers to the point T in Fig. 24. The motion is neutrally stable when linear, and has an amplitude of 2·33° in yaw at a period of 268 sec in the presence of gyro thresholds.

All the response records taken indicate that an approximate stability boundary based on the theory given in Appendix IV is a reliable guide to choosing good combinations of time constants T_c, T_a, τ_2 and τ_3. Provided the linear system is reasonably stable the amplitude forced by autopilot rate-gyro thresholds will be of the same order of magnitude as that obtained on an East/West heading.

In practice difficulty might be encountered in realising very large time constants τ_2 and τ_3 with consistency and reliability if large capacitances are required. High aircraft speeds demand large time constants, as suggested by Fig. 27 where stability boundaries are given for V = 870, 1305, 1740 ft/sec or M = 0·9, 1·35, 1·8 above the tropopause. If the combination τ_2 = 100, τ_3 = 500 is taken as reasonable for the lowest speed, the curves suggest empirically that τ_2 must be increased linearly with V and τ_3 roughly with V^2 in order to continue enforcing stability at the higher speeds.

Fig. 28 depicts approximate stability boundaries for a Type 2 autopilot with crossfeed ratios of 1 and 4, T_1 = 33 sec, and for T_c = 30 sec, V = 870 ft/sec, tan δ = 3. There is little difference between these boundaries and the one marked (a) in Fig. 24 for the Type 1 autopilot. The vertical asymptotes are in fact identical. The combination τ_2 = 100, τ_3 = 500 is thus indicated as a stabilizing one for both types of autopilot in these conditions.

The response records given in Figs. 29 and 30 show that the combination τ_2 = 100, τ_3 = 500 does give a stable motion when the vertical gyro is unmonitored, when it has linear erection with T_1 = 33, and also when it has bang-bang erection with C_ϕ = 2·5 deg/min.

6.4.1. *Turn errors.*—In turning flight the azimuth gyro will be precessed away from its datum because of detector tilt errors. In addition, unless the gyro is on a stabilized platform, the compass indication will have an error because the gimbal rings do not remain orthogonal when the aeroplane is banked[1]. However, any gimballing error is removed as soon as the bank angle returns to zero, whereas the precessional error can only be reduced gradually through the action of the monitor. For slow turns the precessional error is much larger than the gimballing error.

In a steady turn with zero side force the detector tilt is equal to the bank angle. Within the linear range the azimuth gyro will be precessed at a rate

$$\dot{\psi}_c = -f,$$

where $T_c f = \cos\psi \sec(\psi - \psi_m) \sin(\psi_c - \psi_m)$, and the detector error ψ_m is given by the accurate formula stated in Section 3.1. As already explained the precession rate cannot exceed some limiting value in the region of 3 deg/min.

If gimballing errors are neglected the turn error is computed merely by step-by-step integration of the above $\dot{\psi}_c$ equation, and this has been done for one of the cases considered by Stevenson and Lewis[7]. It was assumed that the aeroplane acquires a bank angle of 10° and a rate of turn of 1 deg/sec instantaneously at t = 0, ψ = 90° and that bank angle and rate of turn revert instantaneously to zero when ψ reaches 240°. The result is shown as curve (a) in Fig. 31. Almost from the first instant

the precession signal is large enough to demand the limiting precession rate, which was taken to be 3 deg/min. The decay of the error to zero following the end of the turn is determined by the time constant T_c, in this case 60 sec. Almost identical curves would be obtained for any combination of bank angle and dip angle demanding the limiting precession rate for most of the turning time.

Curve (b) shows the variation in the error when the Sperry modification is introduced into the amplifier. The precession rate is now

$$\dot{\psi}_c = -\frac{1 + \tau_2 D}{1 + \tau_3 D} f$$

within the linear region. In the specific scheme described in Ref. 7 an additional limiter was introduced on the signal f before it passed through the filter producing the transfer function $(1+\tau_2 D)/(1+\tau_3 D)$, and the limiting value was 3 deg/min.

Curve (c) shows what happens if this limiter is omitted, and it is seen that the action of the limiter is to prevent the demand for the maximum precession rate. Again, many combinations of bank angle and dip angle will result in almost identical curves.

For cases (b) and (c) the decay of the error following the end of the turn is determined by the time constant T_c and by the filter modification. It can be shown that the filter modifies the response to a step input to be approximately the same as would be obtained in an unmodified system having a time constant of about $1{\cdot}6\ T_c$.

The magnitude of the turn error, and the time taken after the end of a turn for the error to become small, are additional factors to be weighed when a stabilizing scheme is assessed.

The additional limiter proposed by Sperry was not included in the stability investigation described in this report. It has been shown that the Sperry transfer-function modification can always ensure stable motion and any limit cycle has a small amplitude. In these circumstances the additional limiter would have little effect.

7. *Discussion.*

The theoretical investigation reveals one major cause of oscillatory behaviour on Northerly headings. If the magnetic detector is susceptible to error when tilted roll-wise from the horizontal, a linear system is unstable if the azimuth gyro is monitored too strongly by the detector, or if the autopilot includes a monitor that is too strong, or if the two monitors are too strong a combination. The critical values are determined by aircraft speed and by the sensitivity of the detector to tilting in roll. This sensitivity is approximately proportional to the tangent of the magnetic-dip angle and thus varies with latitude, and also depends on aircraft heading, being a maximum on magnetic North and zero on East/West.

It is worth mentioning that the detector will likewise have a maximum sensitivity to pitch-wise tilt on East/West headings and zero on North. However, there is no direct closed dynamic loop whereby the compass errors react through the pilot on the aircraft motion. If the aeroplane oscillates in pitch there will be oscillatory compass errors, but the treatment for this is to improve the basic control system in pitch.

A real system may be unstable at small amplitudes within a linear region, but the oscillation will grow until it settles down at some particular amplitude which is determined largely by non-linearities such as a limitation of the available precession torque on the azimuth gyro. There can therefore be two approaches to the problem of improving the performance. One is to try and make the system

stable within the linear region; the other is to accept the basic instability but attempt to reduce the amplitude of the limit-cycle oscillation. The second method seems potentially risky in that the system is at the mercy of the non-linearities, and these may vary significantly in different equipments in different aeroplanes. For this reason the investigation was concentrated on the first method.

There are, however, properties such as rate-gyro thresholds which make the system non-linear at very small amplitudes, so that there is still a residual oscillation even though the system is stable in the linear region. Final judgment must therefore be made on the basis of dynamic response, although an analysis of linear-system stability is immensely useful.

To illustrate the order of magnitude of time constants involved, the approximate conditions for stability on a North heading are repeated here:

Type 1 *autopilot*

$$\bar{T}_a + \bar{T}_c - c \tan \delta > \frac{\bar{T}_c}{1 + \bar{T}_c}. \tag{15}$$

Type 2 *autopilot*

$$1 + \bar{T}_c - c \tan \delta > \frac{\bar{T}_c}{\bar{T}_c + \bar{T}_1 - c \tan \delta}. \tag{20}$$

The time constants T_a, T_c, T_1 are expressed as fractions $\bar{T}_a$, etc. of a special time unit $t_1 = T/c$ (i.e. $\bar{T}_a = T_a/t_1$), where T is an aircraft characteristic time equal to V/g, the speed divided by gravitational acceleration. This quantity T is a predominant parameter. The azimuth gyro is monitored through a time constant T_c which has a typical value of 30 sec. Type 1 autopilot uses roll and yaw rate gyros with compass monitoring through a time constant T_a having a typical value of 25 sec. Type 2 autopilot makes direct use of the azimuth gyro and of a vertical gyro monitored from a pendulum through a time constant T_1 having a typical value of 25 sec. The crossfeed ratio c defines the relative strength of yaw and roll signals in the autopilot aileron channel and has a typical value of 1 for a Type 1 autopilot but may be as much as 4 for a Type 2.

For a speed of $M = 0{\cdot}9$ at high altitude, $V = 870$ ft/sec and the characteristic time T is 27 sec. We thus have $\bar{T}_a = 25/27$, $\bar{T}_c = 30/27$, $\bar{T}_1 = 25/27$ as typical values, and expressions (15) and (20) predict that a stable system is not obtained unless tan δ is quite small. Stability can be ensured by weakening the magnetic monitoring, that is by increasing the time constant T_c. Fig. 5 shows that for tan $\delta = 3$, which is appropriate for a latitude of about 58°, T_c would have to be greater than about 75 sec with a Type 1 autopilot having $c = 1$. This represents precessing the azimuth gyro at $0{\cdot}8$ deg/min per degree. Fig. 8 shows that for a Type 2 autopilot having $c = 2$, T_c would have to be greater than about 110 seconds (equivalent to $0{\cdot}545$ deg/min per degree). Improvements can also be effected by increasing T_a or T_1.

An increase in T_c would reduce the accuracy with which the compass is tied to the magnetic datum. An increase in T_1 would reduce the accuracy with which the vertical gyro is held to the pendulum datum. An increase in T_a would reduce the accuracy with which a Type 1 autopilot flies the aircraft on a selected compass heading. Since the selected compass heading can usually be readjusted, the latter discrepancy may not be important, whereas the azimuth and vertical gyros are basic sources of information in the aircraft and must achieve a prescribed performance.

The attractive way of preventing Northerly-heading oscillations is to employ an azimuth gyro so good that small datum errors are achieved even with a monitor time constant sufficiently large to ensure stability. In this way an all-round improvement in compass accuracy should result—not

merely on Northerly headings. The other fundamental cure is to monitor the gyro from a sensor (magnetic or otherwise) that is unaffected or less affected by aircraft tilt. In the past the magnetic detector has been installed far out in a wing in order to minimise magnetic interference from the aeroplane structure or contents, and this has made it too difficult to stabilize the detector except by making it pendulous. The investigation has shown that this crude form of stabilization has negligible influence on Northerly-heading instability. The degree of stabilization required has not been studied, but it is clear that any scheme using a vertical gyro with pendulum monitoring will not be effective unless the pendulum-monitor time constant is large.

Another method of improving Northerly-heading performance is to modify the compass precession signal. Five types of modification have been examined and two of them may be acceptable, namely the R.A.E. and Sperry schemes described in Sections 6.3 and 6.4.

The R.A.E. proposal is to add a yaw rate-gyro component to the compass precession signal with the intention of cancelling the false signal introduced by the magnetic detector when the aeroplane is tilted in roll. Exact cancellation is theoretically achieved if the azimuth gyro is precessed at an additional rate equal to $T \tan \delta / T_c$, on the assumption that the long-period aeroplane motion consists of turns with zero side force. The ideal cancelling signal is proportional to bank angle, but this is not available without a first-class roll datum since a vertical gyro with pendulum monitor would substantially follow the apparent gravity vector unless the monitor strength were very low.

Complications arise in the practical realisation of the R.A.E. scheme on account of rate-gyro thresholds and also the necessity to filter out rate-of-yaw contributions due to the aircraft short-period yawing oscillation. However, it seems possible to effect a considerable improvement with a rate gyro whose threshold is about 0·25 deg/min, and whose signal passes through a one-stage filter with a time constant of about 5 seconds.

The Sperry proposal is to introduce a passive network in the precession amplifier, so that the precession signal is subject to a transfer function $(1 + \tau_2 D)/(1 + \tau_3 D)$, and at the same time modifying the precession time constant T_c if necessary. Increasing this time constant results in proportionally larger steady-state errors due to drift.

It is shown that values of $\tau_2 = 150$, $\tau_3 = 300$ sec as originally suggested are satisfactory at a speed of 870 ft/sec provided T_c is about 60 seconds: this implies doubling the steady-state error as compared with $T_c = 30$ sec. It seems, however, that the combination $\tau_2 = 100$, $\tau_3 = 500$ sec is satisfactory when $T_c = 30$ sec. With higher aircraft speeds the values of τ_2 and τ_3 become larger (*see* Fig. 27), and practical difficulties might arise in getting these time constants.

Another factor is the influence of the Sperry transfer function on the decay of a turn error, but it has been shown that an additional limiter in the amplifier (as also proposed by the firm) in fact ensures smaller errors than obtained in the standard system during a turn. The error developed in the standard system, however, decays more rapidly after the turn is ended, and after a certain time the modified system is holding on larger errors.

8. *Conclusions.*

(*a*) If a gyro-magnetic compass provides the heading reference for the autopilot, the motion of the aeroplane will be basically unstable unless certain monitor time constants are large enough in relation to an aircraft characteristic time equal to the speed divided by gravitational acceleration. Since the available compass-gyro precession torque is limited the aeroplane will settle down to a

constant amplitude oscillation. The larger the magnetic-dip angle and the nearer the heading is to magnetic North then the larger the time constants must be in order to produce a stable system.

(*b*) Monitors are introduced for restricting steady-state errors to small values. The direct way of stabilizing the system by having larger time constants may therefore be unacceptable, since the steady-state errors would be proportionally increased. This approach, however, would be satisfactory if large time constants were permissible on account of the high quality of the equipment. Having a very good azimuth gyro is in principle the simplest way of ensuring stability and small errors.

(*c*) A given unstable standard system can theoretically be made stable in several ways by modifying the precession torque either by introducing an extra signal or a passive network. Some modifications increase the steady-state errors by large factors and this precludes their use, but two schemes were found which might be acceptable.

Acknowledgements.

We wish to acknowledge helpful criticisms and suggestions from Mr. J. F. Green and Mr. C. F. Stone at Smiths Aircraft Instruments Limited, Mr. A. I. Stevenson and Mr. B. F. Lewis of the Sperry Gyroscope Company, Mr. E. G. Goody of A. & A.E.E., and Mr. T. F. Harle of R.A.E. We are also indebted to the Controller of H.M.S.O. and to the Hydrographer of the Navy for permission to reproduce the charts given in Figs. 32 and 33.

LIST OF SYMBOLS

A		Moment of inertia about x axis
b		Wing span
C		Moment of inertia about z axis
C_L		Lift coefficient
c		Crossfeed ratio of autopilot aileron channel (*see* Section 3.2)
D	$=$	d/dt } differential operators
$\overline{D}$	$=$	$t_1 D$ } differential operators
d_a		Drift in autopilot aileron channel
d_b		Threshold of stabilizing rate gyro
d_c		Drift in azimuth-gyro system
E	$=$	$\overline{T}_1 - c \tan \delta$
F		Autopilot aileron gearing
g		Acceleration due to gravity
H		Horizontal intensity of earth's magnetic field
H_1		Autopilot rudder gearing (yaw rate)
H_2		Autopilot rudder gearing (side force)
h		Ratio of stability-equation coefficients, J_1/J_3
i_A		Aircraft inertia coefficient (roll)
i_C		Aircraft inertia coefficient (yaw)
$J_0 \ldots J_4$		Coefficients in stability equation
K	$=$	$c \tan \delta$
K_1		Strength of stabilizing signal (Smith scheme)
K_b		Strength of stabilizing signal (R.A.E. scheme)
k	$=$	$\frac{1}{2} C_L$
L		Aerodynamic rolling moment
L_p, L_r, L_v, L_ξ		Rolling-moment derivatives, $\partial L/\partial p$, etc.
$\mathscr{L}, \mathscr{L}_\xi$	$=$	$-\mu_2 l_v/i_A$, $-\mu_2 l_\xi/i_A$
l_p, l_r, l_v		Non-dimensional derivatives
l_1, l_2	$=$	$-l_p/i_A$, l_r/i_A
M		Mach number

m		Aircraft mass
N		Aerodynamic yawing moment
$N_p, N_r, N_v, N_\xi, N_\zeta$		Yawing-moment derivatives, $\partial N/\partial p$, etc.
$\mathcal{N}, \mathcal{N}_\xi, \mathcal{N}_\zeta$	$=$	$\mu_2 n_v/i_c,\ \mu_2 n_\xi/i_c,\ -\mu_2 n_\zeta/i_c$
n_p, n_r, n_v		Non-dimensional derivatives
n_1, n_2	$=$	$-n_p/i_c,\ -n_r/i_c$
P		Period of oscillation
p		Aircraft angular velocity about x axis (roll)
p_a		Roll rate-gyro signal
r		Aircraft angular velocity about z axis (yaw)
r_a		Yaw rate-gyro signal
r_b		Stabilizing rate-gyro signal
S		Wing area
T		Aeroplane characteristic time, V/g
T_1		Pendulum-monitor time constant for vertical gyro (*see* Section 3.2)
T_a		Compass-monitor time constant for autopilot (*see* Section 3.1)
T_c		Magnetic-monitor time constant for compass gyro (*see* Section 3.1)
t_1		Special unit of time, V/gc
$\hat{t}$		Unit of aerodynamic time, $m/\rho SV$
V		True airspeed in undisturbed flight
v		Increment of velocity along y axis
Y		Aerodynamic force along y axis
Y_v, Y_ζ		Side-force derivatives, $\partial Y/\partial v$, etc.
y_v, y_ζ		Non-dimensional derivatives
$\bar{y}_v$	$=$	$-y_v$
α_y		Angle between pendulum and x, z plane (*see* Section 3.2)
δ		Magnetic-dip angle
ϵ		Vertical-gyro error (*see* Section 3.2)
ζ		Increment of rudder deflection
μ_2		Aircraft relative density, $2m/\rho Sb$

LIST OF SYMBOLS—*continued*

ξ	Increment of aileron deflection
ρ	Air density
τ	Filter time constant (*see* Section 6.3)
τ_1	Autopilot rudder-channel time constant (*see* Section 4.2)
τ_2, τ_3	Time constants (*see* Section 6.4)
ϕ	Aircraft bank angle
ϕ_m	Roll-wise tilt of magnetic detector
ψ	Aircraft heading relative to magnetic North
ψ_c	Azimuth-gyro heading relative to magnetic North
ψ_i	Compass indication, $(\psi - \psi_c)$
ψ_m	Magnetic-detector error

Overscript

A bar placed over a symbol denotes that time is being expressed in units of magnitude t_1. Thus $\bar{T} = T/t_1$, $\bar{D} = t_1 D$.

REFERENCES

No.	*Author(s)*	*Title, etc.*
1	I. L. Thomas	The errors of gyroscopically stabilized magnetic compasses in aircraft and the development of a new design to minimise these effects. A.R.C. 13 190. November, 1949.
2	J. F. Green and A. P. Glenny ..	Heading definition in commercial aircraft. *J. Inst. Nav.*, Vol. XIII, No. 2, p. 196. August, 1960.
3	H. R. Hopkin	Routine computing methods for stability and response investigations on linear systems. A.R.C. R. & M. 2392. August, 1946.
4	H. R. Hopkin and H. H. B. M. Thomas	Definitions and terms relating to aircraft control systems and components. *J. R. Ae. Soc.*, Vol. 63, No. 586, p. 572. October, 1959.
5	L. W. Bryant and S. B. Gates ..	Nomenclature for stability coefficients. A.R.C. R. & M. 1801. October, 1937.
6	—	Royal Aeronautical Society Data Sheets, Aerodynamics, Vol. 3. December, 1958.
7	A. I. Stevenson and B. F. Lewis ..	Gyrosyn integral control. Sperry Gyroscope Co. Tech. Note No. 270. November, 1957.

APPENDIX I

Non-Dimensional Aerodynamic Derivatives

The following relations exist between derivatives measured in ordinary units and denoted by capital letters and their non-dimensional counterparts defined by Bryant and Gates[5] in R. & M. 1801 and denoted by small letters. These are also listed in the R.Ae.S. Data Sheets[6]

$$\frac{Y_v}{y_v} = \frac{2L_v}{bl_v} = \frac{2N_v}{bn_v} = \rho SV,$$

$$\frac{L_p}{l_p} = \frac{L_r}{l_r} = \frac{N_p}{n_p} = \frac{N_r}{n_r} = \tfrac{1}{4}\rho SVb^2,$$

$$\frac{L_\xi}{l_\xi} = \frac{N_\xi}{n_\xi} = \frac{N_\zeta}{n_\zeta} = \tfrac{1}{2}\rho SV^2 b,$$

$$\frac{Y_\zeta}{y_\zeta} = \rho SV^2,$$

where S is the wing area, V is the steady speed in undisturbed flight, b is the wing span, and ρ is the air density.

APPENDIX II

Normalised Equations of Motion

The lateral equations of motion in normalised (often called non-dimensional) form may be written as

$$(\hat{D}+\bar{y}_v)\hat{v} - k\phi + \hat{r} - y_\zeta\zeta = 0,$$

$$\mathscr{L}\hat{v} + (\hat{D}+l_1)\hat{p} - l_2\hat{r} + \mathscr{L}_\xi\xi = 0,$$

$$-\mathscr{N}\hat{v} + n_1\hat{p} + (\hat{D}+n_2)\hat{r} - \mathscr{N}_\xi\xi + \mathscr{N}_\zeta\zeta = 0,$$

where

$$\bar{y}_v = -y_v,$$

$$k = \tfrac{1}{2}C_L = 2mg/\rho SV^2,$$

$$\frac{\mathscr{L}}{-l_v} = \frac{\mathscr{L}_\xi}{-l_\xi} = \frac{\mu_2}{i_A},$$

$$\frac{\mathscr{N}}{n_v} = \frac{\mathscr{N}_\xi}{n_\xi} = \frac{\mathscr{N}_\zeta}{-n_\zeta} = \frac{\mu_2}{i_c},$$

$$\frac{l_1}{-l_p} = \frac{l_2}{l_r} = \frac{1}{i_A},$$

$$\frac{n_1}{-n_p} = \frac{n_2}{-n_r} = \frac{1}{i_c},$$

$$\frac{i_A}{A} = \frac{i_c}{C} = \frac{4}{mb^2},$$

$$\hat{D} = \hat{t}D,$$

$$\hat{v} = v/V,$$

$$\hat{p} = \hat{t}p,$$

$$\hat{r} = \hat{t}r,$$

and

$\mu_2 = 2m/\rho Sb$, the relative-density parameter,

$\hat{t} = m/\rho SV$, a quantity having the dimensions of time.

It is convenient to regard the variables $\hat{v}$, $\hat{p}$, $\hat{r}$ as the values of v, p, r expressed in a special system of units in which the unit of speed is V, the unit of time is $\hat{t}$, and the unit of mass is m. In these units time is measured in airsec.

The autopilot equations (30), (34), and the compass equation (35) expressed in these units become

$$\hat{D}\xi = F\left[\hat{p}_a + c\hat{r}_a + \frac{c}{\hat{T}_a}(\psi - \psi_c)\right], \tag{30a}$$

$$\hat{D}\zeta = \hat{H}_1\hat{D}\hat{r}_a + \hat{H}_2\alpha_y, \tag{34a}$$

where

$$\alpha_y = \frac{y_v\hat{v} + y_\zeta\zeta}{k},$$

$$\hat{H}_1 = H_1/\hat{t},$$

$$\hat{H}_2 = H_2\hat{t},$$

and

$$\hat{T}_c\hat{D}\psi_c = \tan\delta\left(\hat{T}\hat{r} + \frac{\hat{D}\hat{v}}{k}\right) - \psi_c, \tag{35a}$$

where

$$\hat{T}_c = T_c/\hat{t},\quad \hat{T} = T/\hat{t}.$$

The vertical-gyro monitor equation (11), which is required with the alternative aileron equation (10), becomes

$$\hat{T}_1\hat{D}\epsilon = \phi - \epsilon + \alpha_y, \tag{11a}$$

where

$$\hat{T}_1 = T_1/\hat{t}.$$

APPENDIX III

Numerical Data

(in notation of Appendices I and II)

	Aeroplane A	Aeroplane B
Altitude (ft)	40,000	40,000
E.A.S. (kt)	256	256
V (ft/sec)	870	870
M	0·9	0·9
C_L	0·113	0·242
μ_2	26·4	165
$\hat{t}$ (sec)	1·51	3·31
l_1	2·5	2·43
l_2	0·365	0·587
$\mathscr{L}$	5·84	247·5
$\mathscr{L}_\xi$	32·24	197
n_1	0	−0·07
n_2	0·237	0·8
$\mathscr{N}$	6·72	44·14
$\mathscr{N}_\xi$	0	−1·24
$\mathscr{N}_\zeta$	3·74	28·9
$\bar{y}_v$	0·148	0·386
y_ζ	0·052	0·0625
k	0·0565	0·121
i_C	0·228	0·4
i_A	0·104	0·092
$\hat{H}_1$	0·662	0·302
$\hat{H}_2$	2·14	2·19
F	1·0	1·0
T (sec)	27	27

(88992)

APPENDIX IV

Approximate Theory of Sperry and A. & A.E.E. Modified Systems with Type 1 Autopilot

1. *Sperry System.*

The Sperry precession equation for the azimuth gyro is (within the linear range)

$$T_c D\psi_c = \frac{1+\tau_2 D}{1+\tau_3 D}(T\tan\delta\ D\psi - \psi_c), \tag{40}$$

if we take the unmodified equation to be (6). When $\tau_2 = 0$ equation (40) is valid for the A. & A.E.E. modified system.

Choosing a time unit $t_1 = T/c$ as in Section 3.2, we can write (40) as

$$\bar{T}_c \bar{D}\psi_c = \frac{1+\bar{\tau}_2\bar{D}}{1+\bar{\tau}_3\bar{D}}(c\tan\delta\ \bar{D}\psi - \psi_c), \tag{40a}$$

where

$$\bar{\tau}_2 = \tau_2/t_1,\ \bar{\tau}_3 = \tau_3/t_1.$$

Combining this equation with the aircraft autopilot equation (13), we obtain a fourth-order equation

$$J_4\bar{D}^4\psi + J_3\bar{D}^3\psi + J_2\bar{D}^2\psi + J_1\bar{D}\psi + J_0\psi = 0, \tag{41}$$

where

$$\begin{aligned} J_4 &= \bar{T}_a\bar{T}_c\bar{\tau}_3, \\ J_3 &= \bar{T}_a(\bar{T}_c + \bar{\tau}_2 + \bar{T}_c\bar{\tau}_3) \\ J_2 &= \bar{T}_a(1+\bar{T}_c+\bar{\tau}_2) + \bar{T}_c\bar{\tau}_3 - \bar{\tau}_2 c\tan\delta, \\ J_1 &= \bar{T}_a + \bar{T}_c + \bar{\tau}_2 - c\tan\delta, \\ J_0 &= 1. \end{aligned}$$

If $\tau_2 = \tau_3 = 0$, or if $\tau_2 = \tau_3 = \infty$, there is a reversion to the third-order equation (14).

One immediate conclusion from the form of these coefficients is that if the standard system has $\bar{T}_a + \bar{T}_c < c\tan\delta$, then J_1 will remain negative (and the modified system will be unstable) if $\tau_2 = 0$. This is so for the A. & A.E.E. modification.

The Sperry modification has $\tau_2 \neq 0$ and it is therefore possible to choose a value to make J_1 and J_2 positive, and it should be noted that increasing τ_2 tends to reduce J_2 unless τ_3 is suitably chosen. If all five coefficients are positive, the remaining Routh-Hurwitz criterion for stability is that

$$J_2 > \frac{h}{J_4} + \frac{J_0}{h},$$

where $h = J_1/J_3$. Since the J coefficients are rather complicated functions of the time constants this stability condition is mainly useful for testing particular numerical values. In order to carry out a more general analysis the locus of zero oscillatory damping may be plotted in the τ_2, τ_3 plane for fixed values of the other quantities. It is convenient to use $\beta = \bar{\omega}^2$ as a parameter, where $\bar{\omega}$ is the angular frequency of the oscillation expressed in terms of the time unit t_1. If ω is the equivalent value in rad/sec, $\bar{\omega} = t_1\omega$. The symbol K, introduced in the following algebra, represents $c\tan\delta$.

An oscillation of frequency $\bar{\omega}$ and with zero damping will result when

$$\left.\begin{aligned}\bar{\tau}_3 &= \frac{1-P_1\beta+P_2\beta^2}{\beta(R_0-R_1\beta+R_2\beta^2)},\\ \bar{\tau}_2 &= \frac{Q_0-Q_1\beta-Q_2\beta^2}{R_0-R_1\beta+R_2\beta^2},\end{aligned}\right\} \tag{42}$$

where

$$\left.\begin{aligned}P_1 &= \bar{T}_a(2K+2-\bar{T}_a)-K(K-\bar{T}_c),\\ P_2 &= \bar{T}_a(\bar{T}_a+K\bar{T}_c),\end{aligned}\right\} \tag{43}$$

$$\left.\begin{aligned}Q_0 &= \bar{T}_c(K-\bar{T}_c),\\ Q_1 &= \bar{T}_a\bar{T}_c(\bar{T}_a\bar{T}_c+K-2\bar{T}_c),\\ Q_2 &= \bar{T}_a{}^2\bar{T}_c{}^2,\end{aligned}\right\} \tag{44}$$

$$\left.\begin{aligned}R_0 &= \bar{T}_c,\\ R_1 &= \bar{T}_a\bar{T}_c(K+2-\bar{T}_a),\\ R_2 &= \bar{T}_c\bar{T}_a{}^2.\end{aligned}\right\} \tag{45}$$

The stability boundary may be plotted by substituting a succession of positive values of β in equations (42). For the orders of magnitude considered, the relevant part of the boundary is in the positive quadrant and is asymptotic to the two straight lines

$$\bar{\tau}_2 = K-\bar{T}_c, \tag{46}$$

$$\beta_1 Q_0'\bar{\tau}_3 = P_0'\bar{\tau}_2+(P_1'Q_0'-P_0'Q_1')/R_1'+P_0'Q_0'/\beta_1R_1', \tag{47}$$

where

$$\begin{aligned}P_0' &= 1-P_1\beta_1+P_2\beta_1{}^2,\\ P_1' &= P_1-2P_2\beta_1,\\ Q_0' &= Q_0-Q_1\beta_1-Q_2\beta_1{}^2,\\ Q_1' &= Q_1+2Q_2\beta_1,\\ R_1' &= R_1-2R_2\beta_1,\end{aligned}$$

and β_1 is the smaller root of

$$R_0-R_1\beta+R_2\beta^2 = 0. \tag{48}$$

Fig. 21 shows the general shape of the stability boundary. The minimum occurs for a frequency corresponding to $\beta = \beta_2$, a root of the equation

$$P_2R_2\beta^4-2P_1R_2\beta^3+(3R_2+P_1R_1-R_0P_2)\beta^2-2R_1\beta+R_0 = 0. \tag{49}$$

For the kind of values considered in this investigation β_1 is small, so that the β^3 and β^4 terms in equation (49) may be neglected with little loss of accuracy. In fact tolerably correct estimates of β_1 and β_2 may be obtained if β^2 terms are neglected, and equations (48) and (49) then give

$$\beta_1 \approx R_0/R_1, \quad \beta_2 \approx 0{\cdot}5\beta_1. \tag{50}$$

It is unwise to use this approximation except for determining roughly the range of values of β to be substituted in equations (42). Thus the values of β_2 given by (50) for the curves (a), (b) and (c) in Fig. 25 are 0·133, 0·0858, 0·133 respectively and these correspond to periods of 466, 580 and 466 sec, whereas the correct values are about 455, 475, 400 sec respectively.

2. *A. & A.E.E. System.*

The equation of motion for the A. & A.E.E. system can be deduced from equation (41) by putting $\tau_2 = 0$. The coefficients are therefore

$$J_4 = \bar{T}_a \bar{T}_c \bar{\tau}_3,$$

$$J_3 = \bar{T}_a \bar{T}_c (1 + \bar{\tau}_3),$$

$$J_2 = \bar{T}_a (1 + \bar{T}_c) + \bar{T}_c \bar{\tau}_3,$$

$$J_1 = \bar{T}_a + \bar{T}_c - c \tan \delta,$$

$$J_0 = 1.$$

It is seen at once that if the unmodified system has $\bar{T}_a + \bar{T}_c < c \tan \delta$ it is unstable and no value of τ_3 can make it stable since J_1 remains negative. If the unmodified system is unstable with $\bar{T}_a + \bar{T}_c > c \tan \delta$, it may be possible to find a value of τ_3 to impose stability. All the coefficients are positive so that the condition for stability is

$$J_2 > \frac{h}{J_4} + \frac{J_0}{h},$$

where $h = J_1/J_3$. This condition is the same as

$$\frac{F_1}{F_3^2 \bar{\tau}_3 (1 + \bar{\tau}_3)} + \bar{\tau}_3 \left(\frac{F_3}{F_1} - \bar{T}_c \right) + \left(\frac{F_3}{F_1} - F_2 \right) < 0, \tag{51}$$

where the F's are the coefficients for the unmodified system, that is $F_3 = \bar{T}_a \bar{T}_c$, $F_2 = \bar{T}_a (1 + \bar{T}_c)$, $F_1 = J_1$. The first and third terms of (51) are positive, and the modified system can therefore be stable only if the second term, which is equal to

$$\frac{\bar{T}_c (c \tan \delta - \bar{T}_c) \bar{\tau}_3}{\bar{T}_a + \bar{T}_c - c \tan \delta},$$

is negative, that is if $\bar{T}_c > c \tan \delta$. This represents a severe limitation.

APPENDIX V

Constants of Earth's Magnetic Field at Greenwich Meridian

(From Admiralty Charts, 1955)

Latitude (deg N)	Dip angle, δ (deg)	tan δ	Horizontal field (c.g.s. units)	Vertical field (c.g.s. units)
0	−22·5	−0·414	0·287	−0·115
10	+ 0·1	+0·002	0·320	+0·008
20	+23·0	+0·425	0·323	+0·136
30	+41·8	+0·894	0·293	+0·264
40	+55·7	+1·47	0·245	+0·360
50	+65·6	+2·20	0·194	+0·428
60	+72·6	+3·19	0·146	+0·470
70	+77·6	+4·55	0·110	+0·500

The above values were obtained from the charts by visual interpolation and the accuracy of the last place of decimals is not guaranteed.

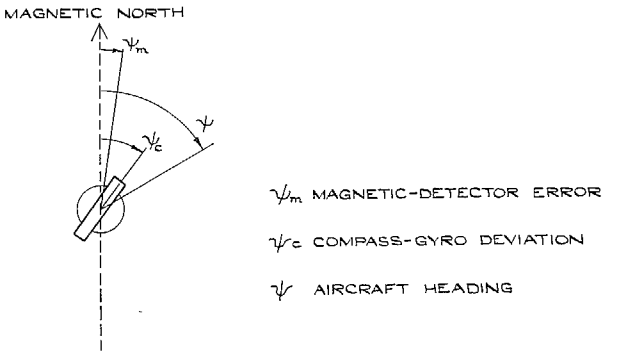

FIG. 1. Definition of azimuth angles.

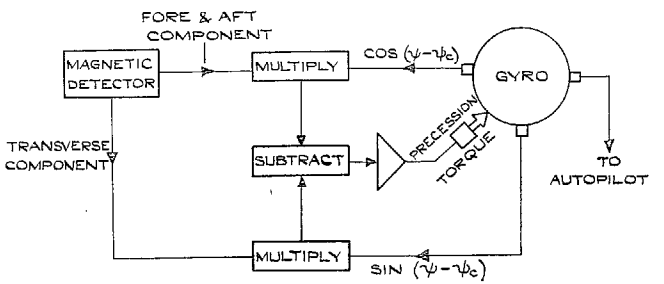

FIG. 2. Block diagram of gyro-magnetic compass.

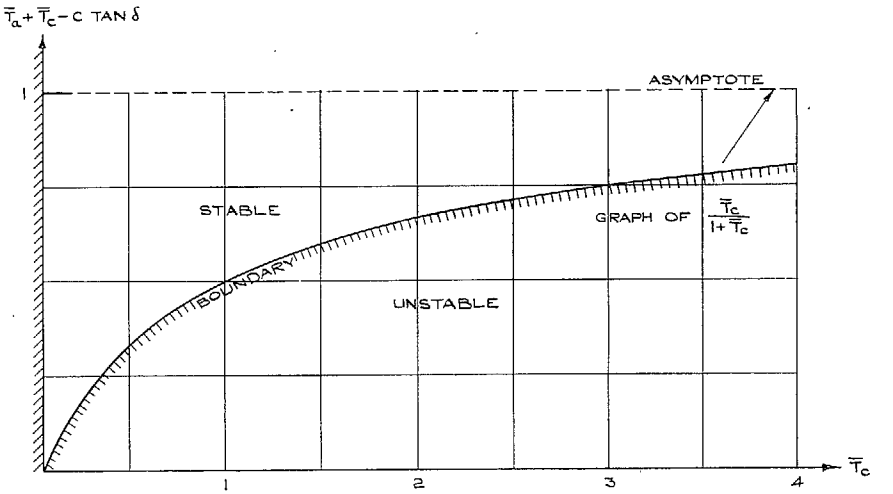

FIG. 3. Approximate stability boundary (Type 1 autopilot).

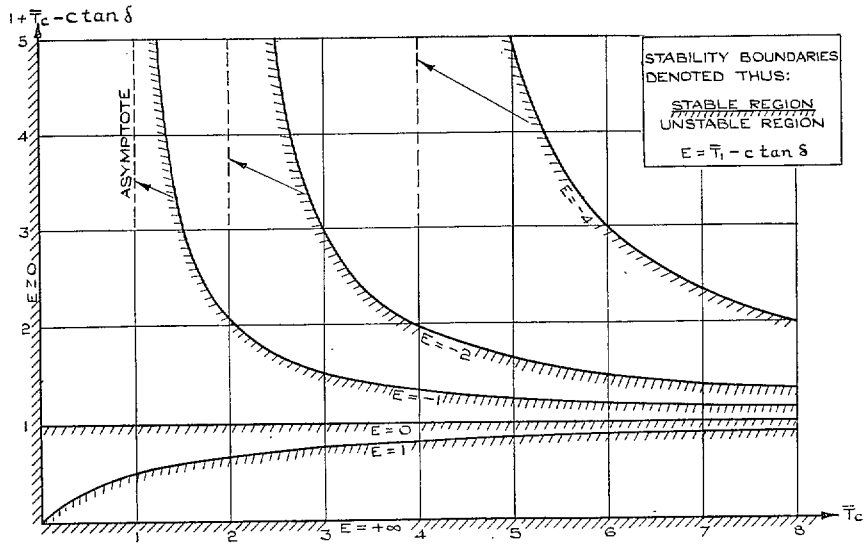

FIG. 4. Approximate stability boundaries (Type 2 autopilot).

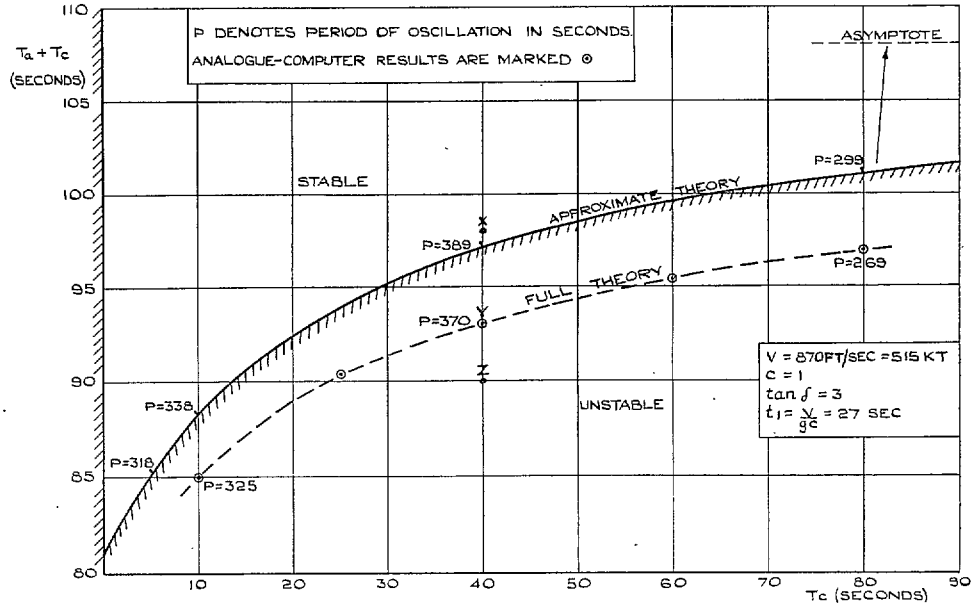

FIG. 5. Comparison of approximate and full-theory stability boundaries (Type 1 autopilot).

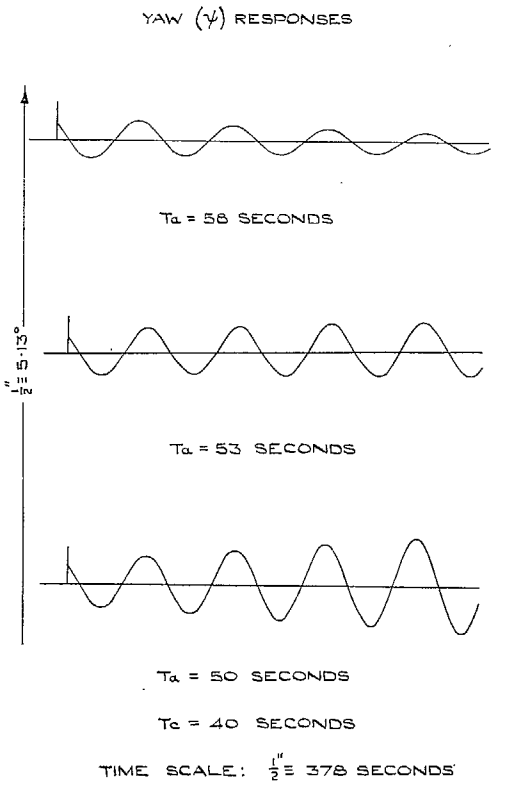

FIG. 6. Records for determining neutral stability conditions.

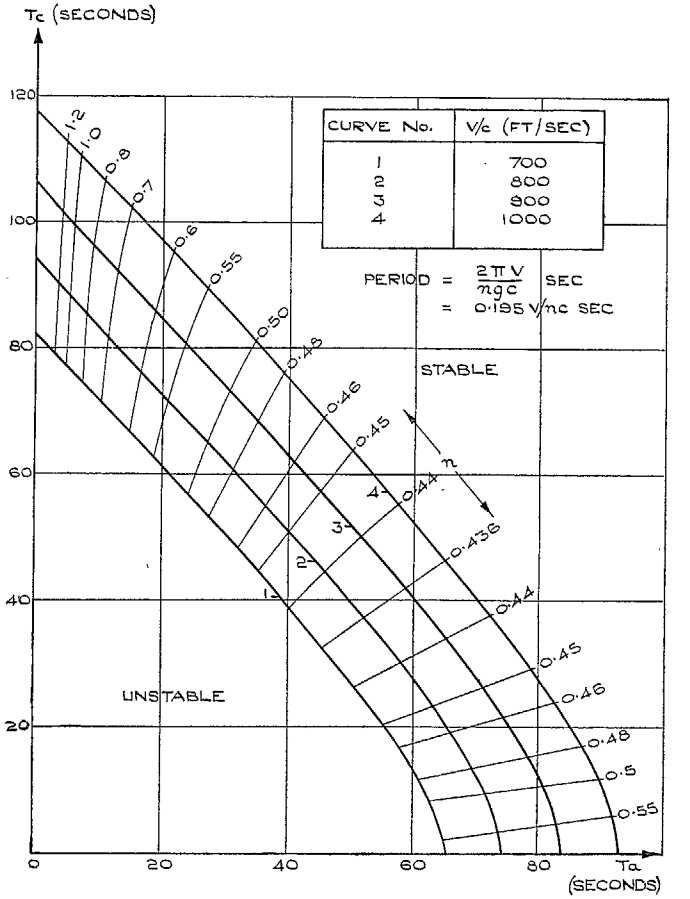

FIG. 7. Approximate stability boundaries (Type 1 autopilot).

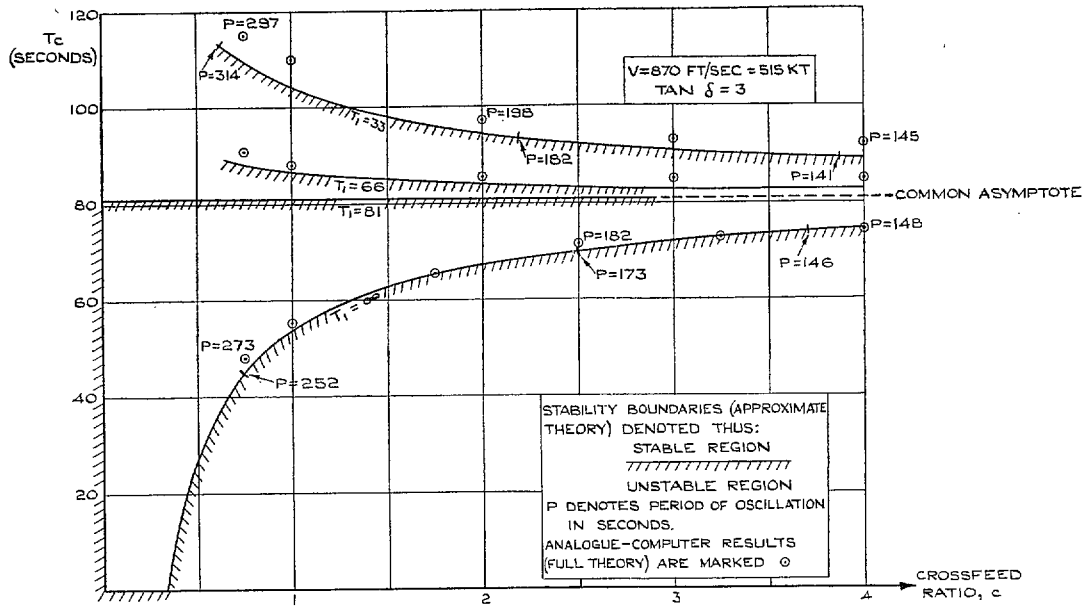

FIG. 8. Comparison of approximate and full-theory stability boundaries (Type 2 autopilot).

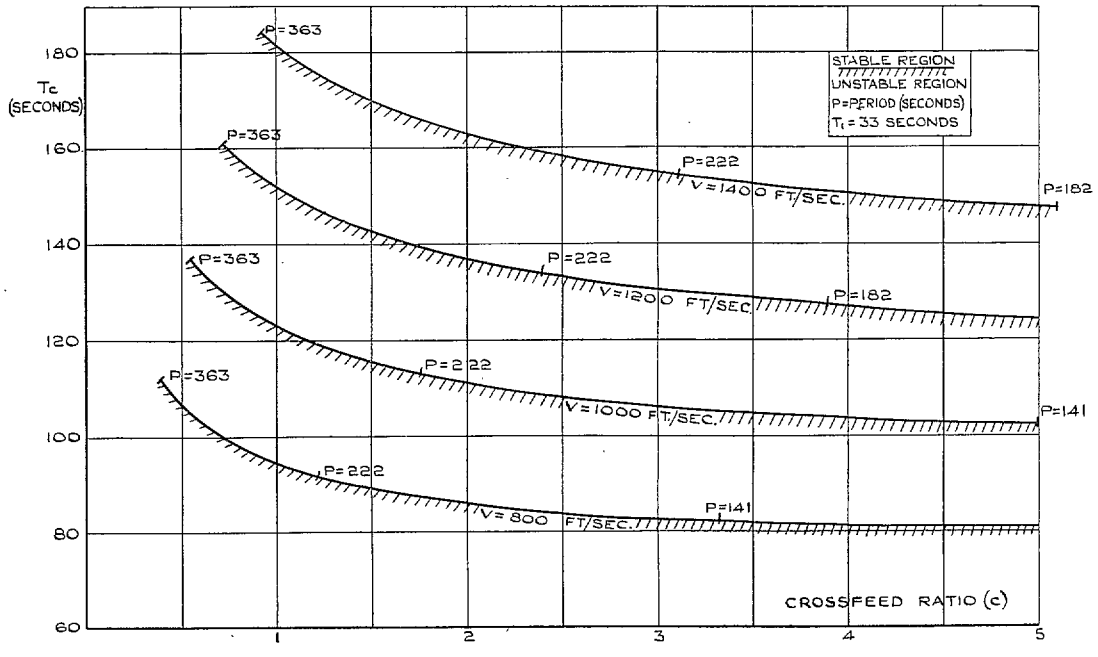

FIG. 9. Approximate stability boundaries (Type 2 autopilot).

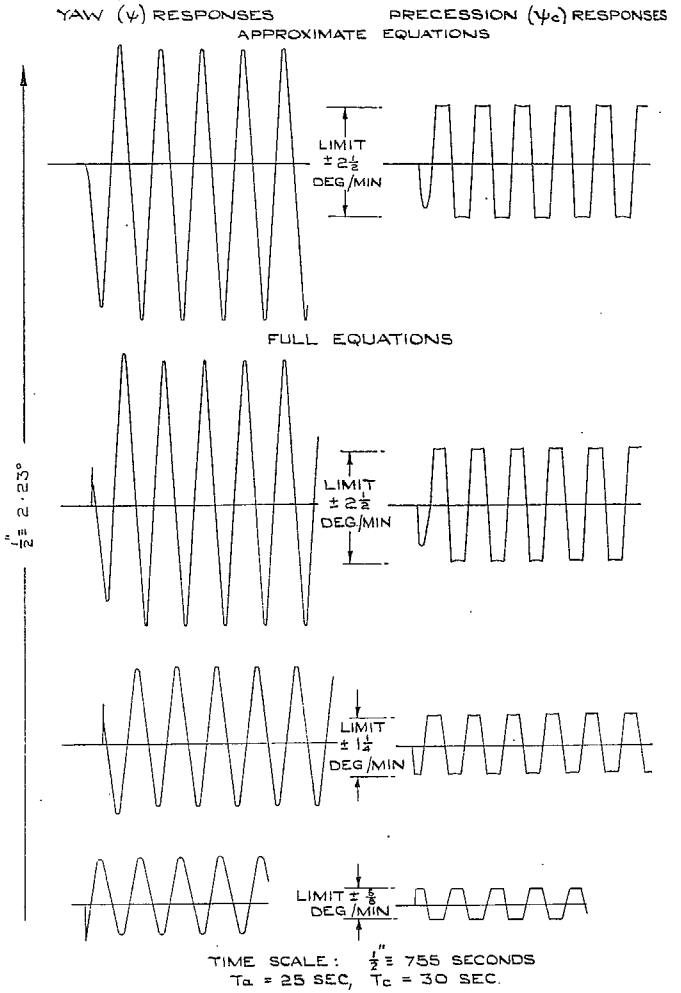

FIG. 10. Effect of limiting precession rate (Type 1 autopilot, Aeroplane A).

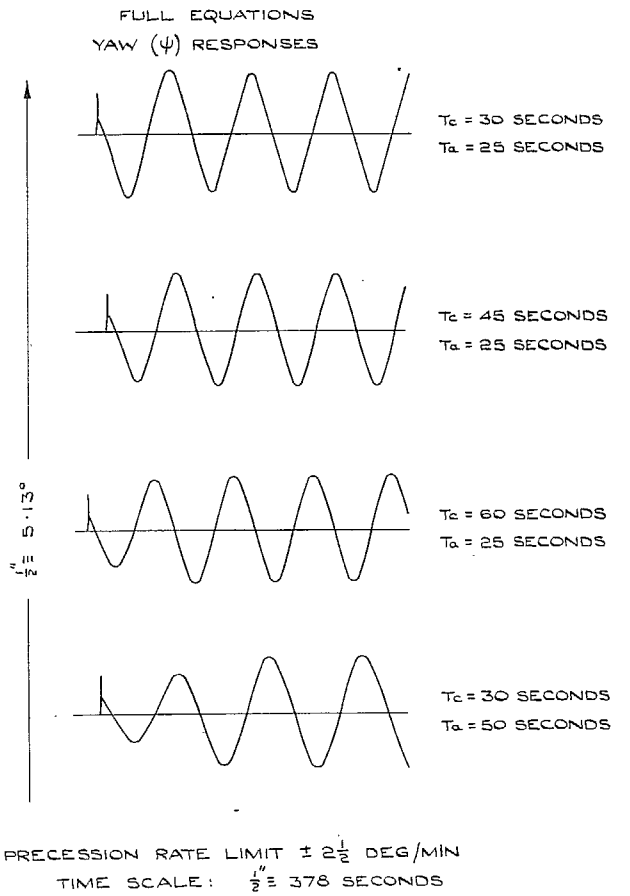

FIG. 11. Effect of limiting precession rate (Type 1 autopilot, Aeroplane A).

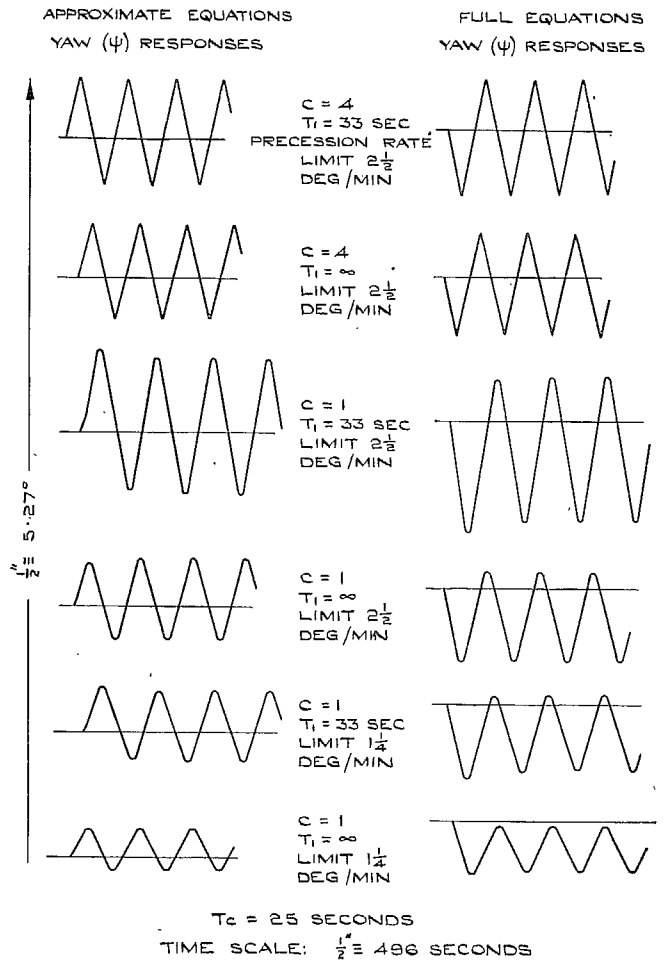

FIG. 12. Effect of limiting precession rate (Type 2 autopilot, aeroplane B).

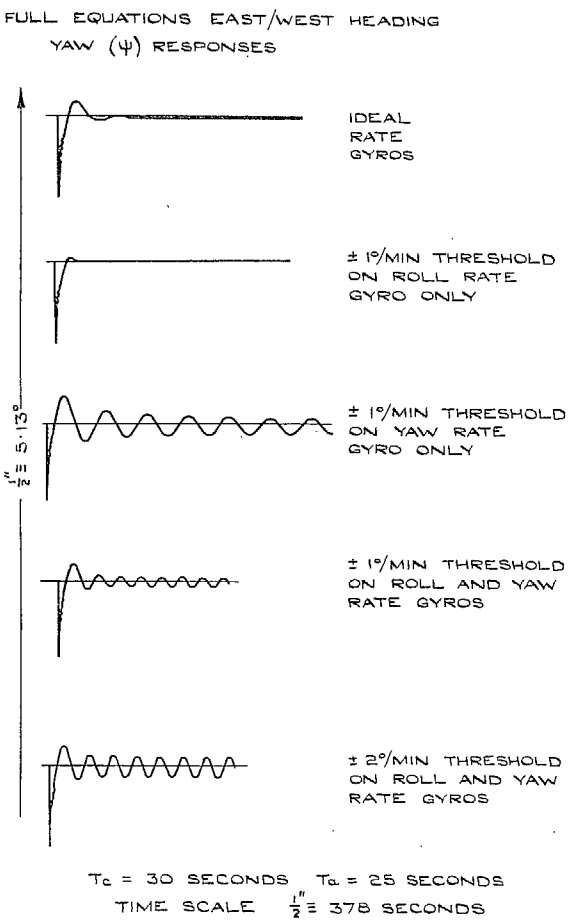

FIG. 13. Effect of autopilot rate-gyro thresholds (Type 1 autopilot, aeroplane A).

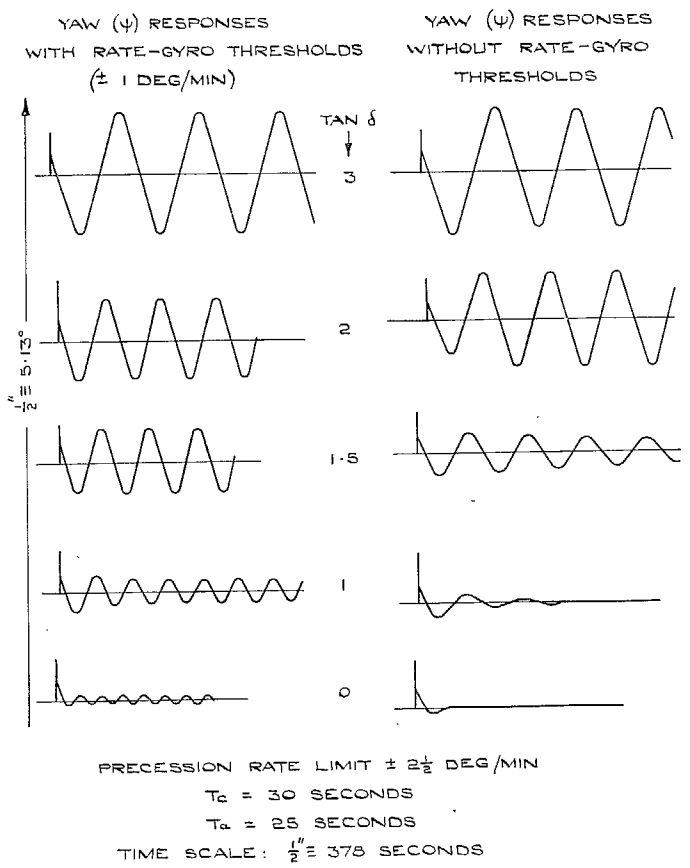

PRECESSION RATE LIMIT ± 2½ DEG/MIN
T_c = 30 SECONDS
T_a = 25 SECONDS
TIME SCALE: ½" ≡ 378 SECONDS

FIG. 14. Effect of varying latitude or heading (Type 1 autopilot, aeroplane A).

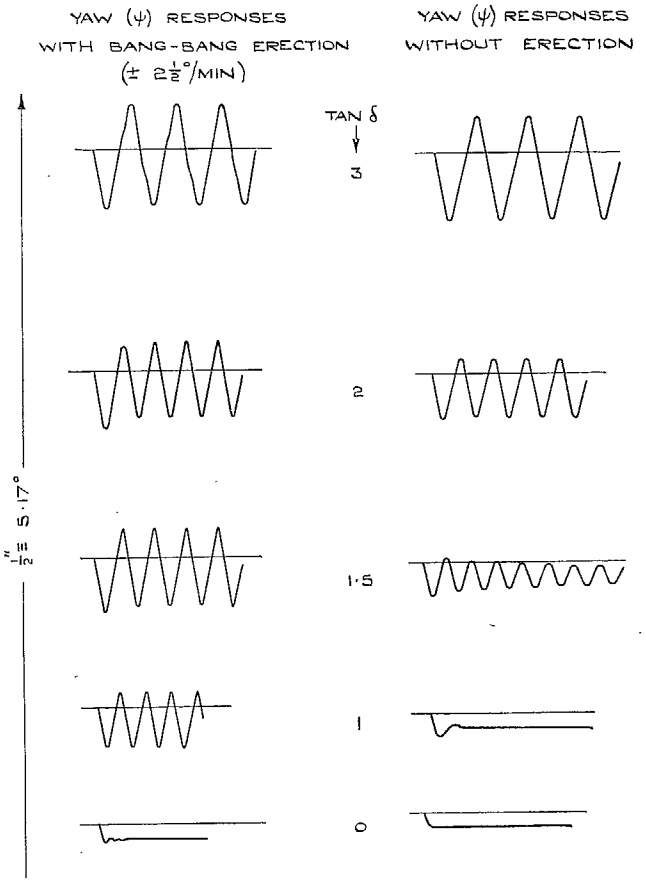

CROSSFEED C = 2
T_c = 30 SECONDS
TIME SCALE: ½" = 496 SECONDS

FIG. 15. Effect of vertical-gyro bang-bang erection (Type 2 autopilot, aeroplane B).

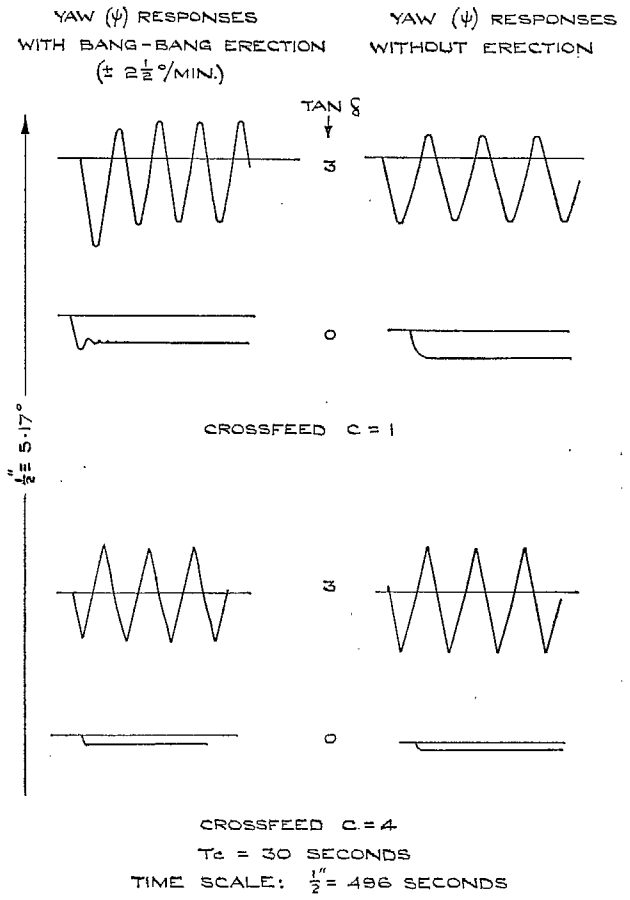

FIG. 16. Effect of vertical-gyro bang-bang erection (Type 2 autopilot, aeroplane B).

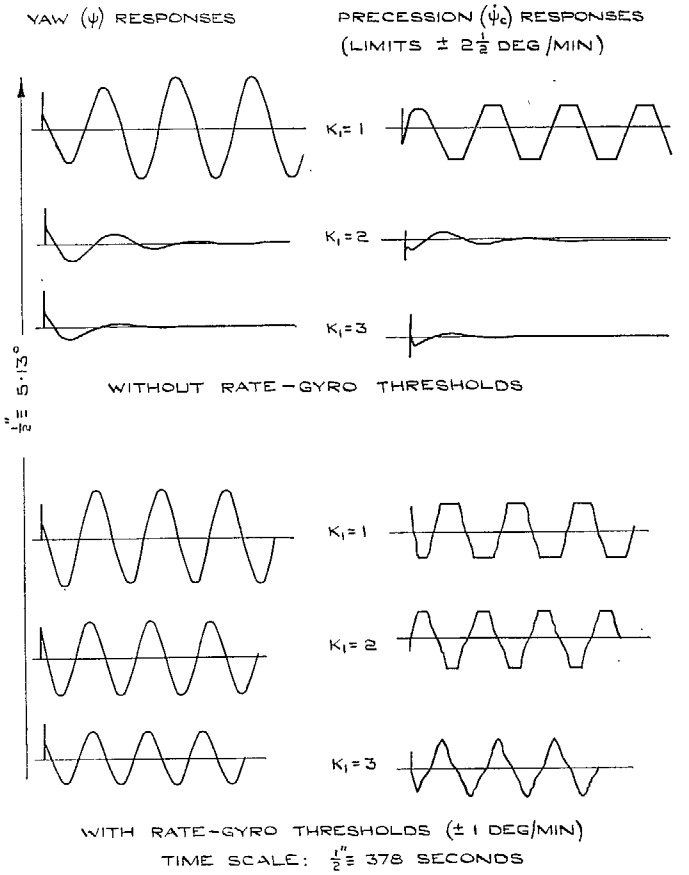

FIG. 17. Augmented-feedback stabilizing scheme (Type 1 autopilot, aeroplane A).

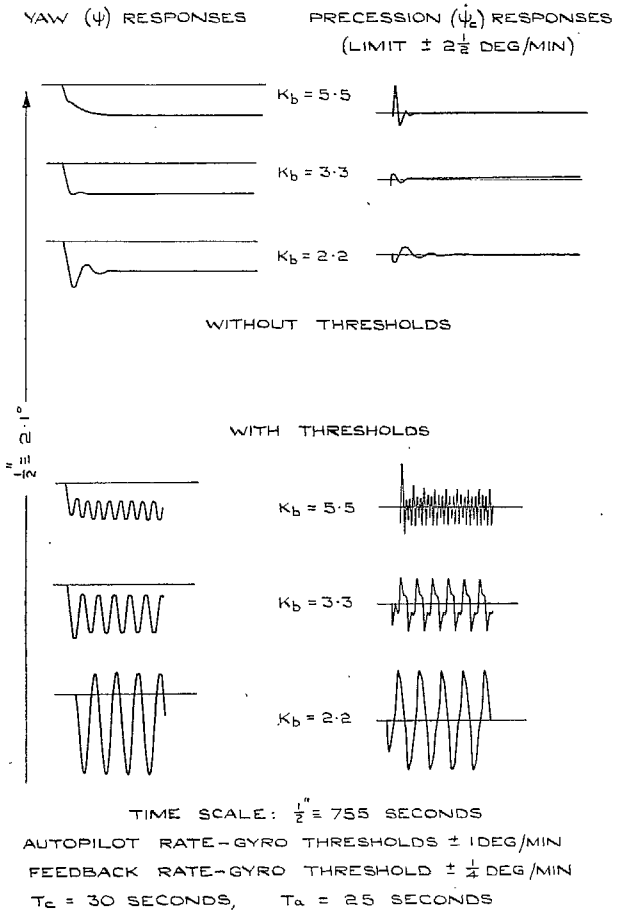

FIG. 18. R.A.E. stabilizing scheme (Type 1 autopilot, aeroplane A).

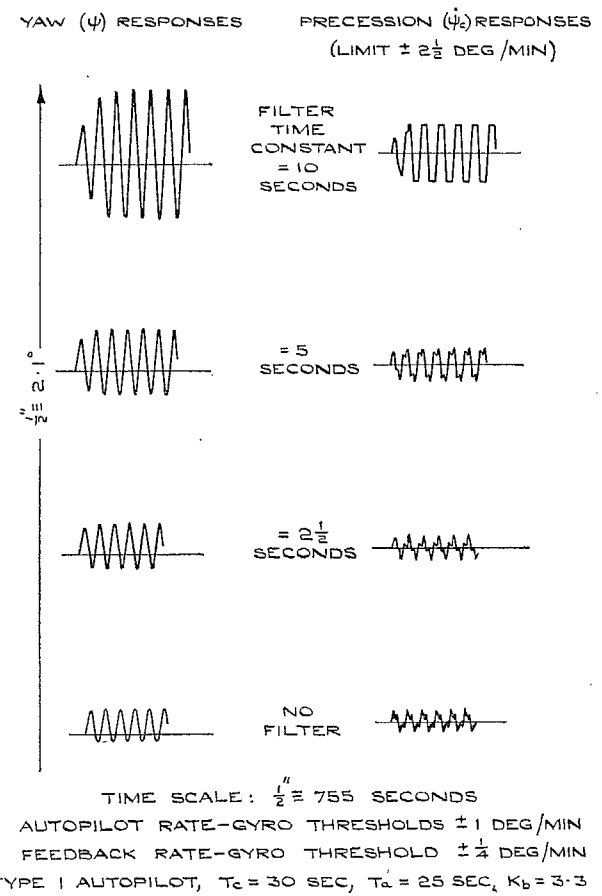

FIG. 19. Effect of filter in rate-gyro feedback on long-period response (R.A.E. scheme).

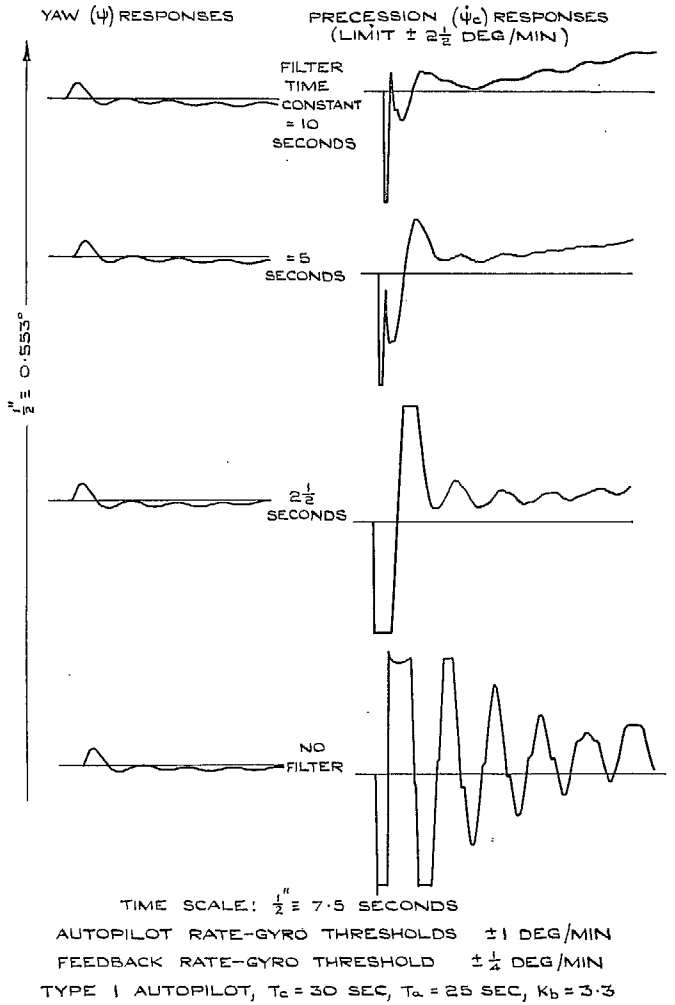

FIG. 20. Effect of filter in rate-gyro feedback on short-period response (R.A.E. scheme).

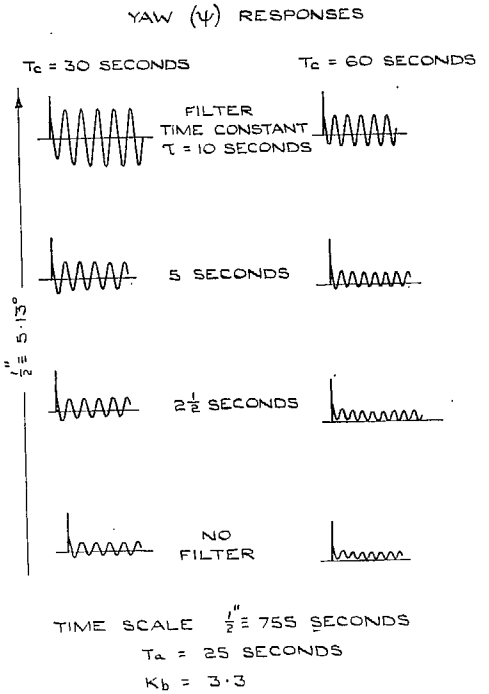

FIG. 21. Effect of changing T_c (R.A.E. scheme).

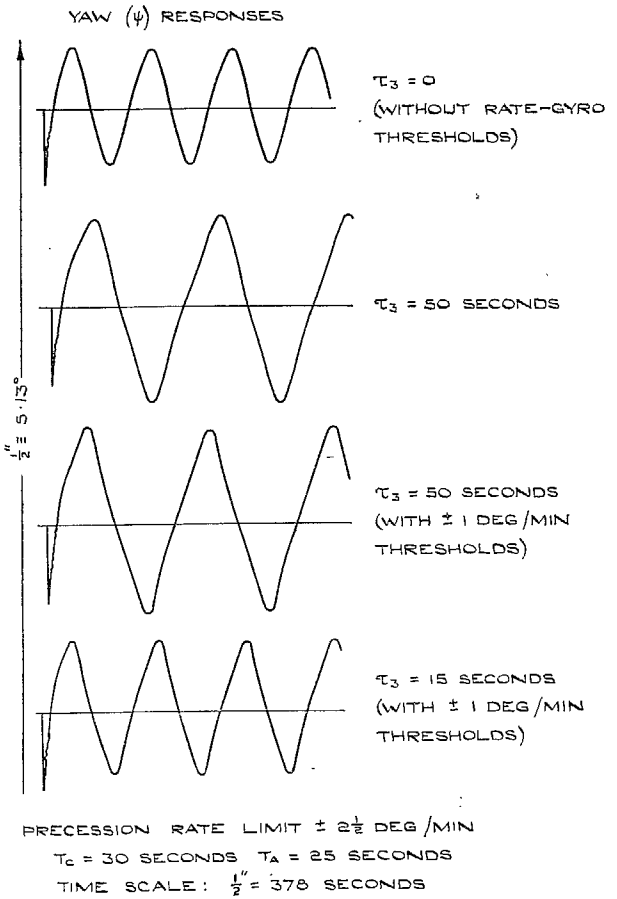

FIG. 22. A. & A.E.E. stabilizing scheme (Type 1 autopilot).

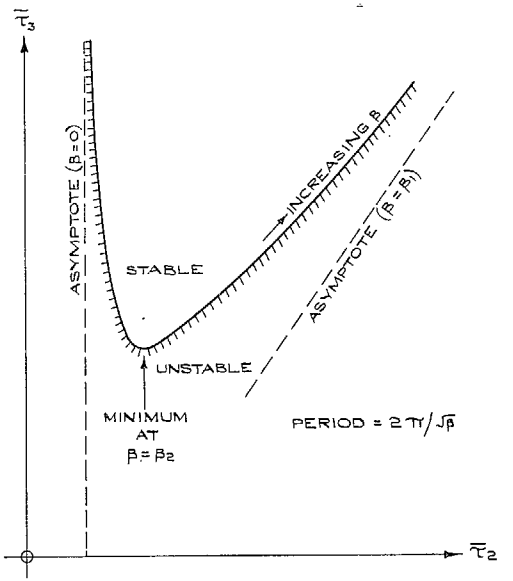

FIG. 23. Sperry stabilizing scheme approximate stability boundary (Type 1 autopilot).

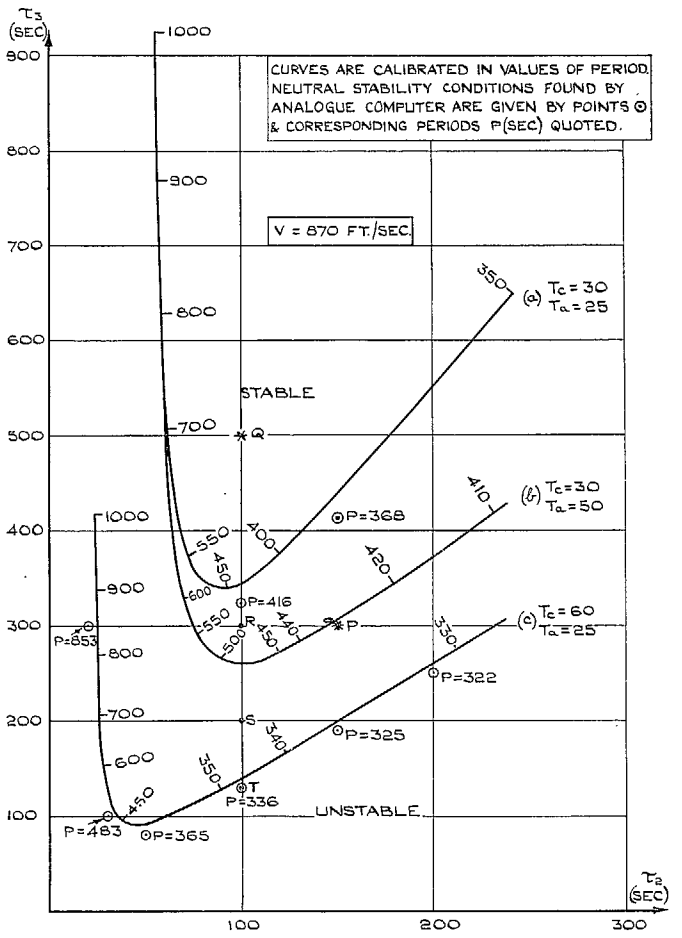

FIG. 24. Sperry stabilizing scheme approximate stability boundaries (Type 1 autopilot).

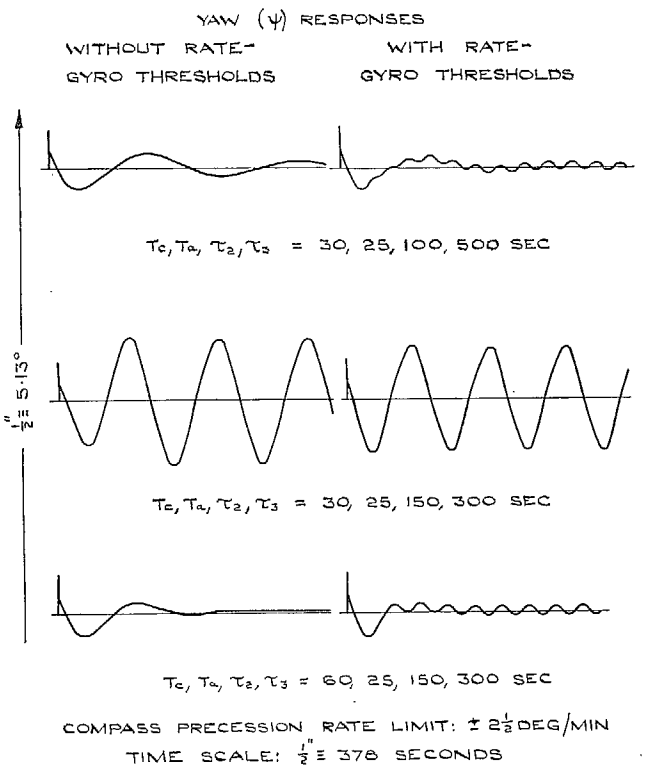

FIG. 25. Sperry stabilizing scheme (Type 1 autopilot).

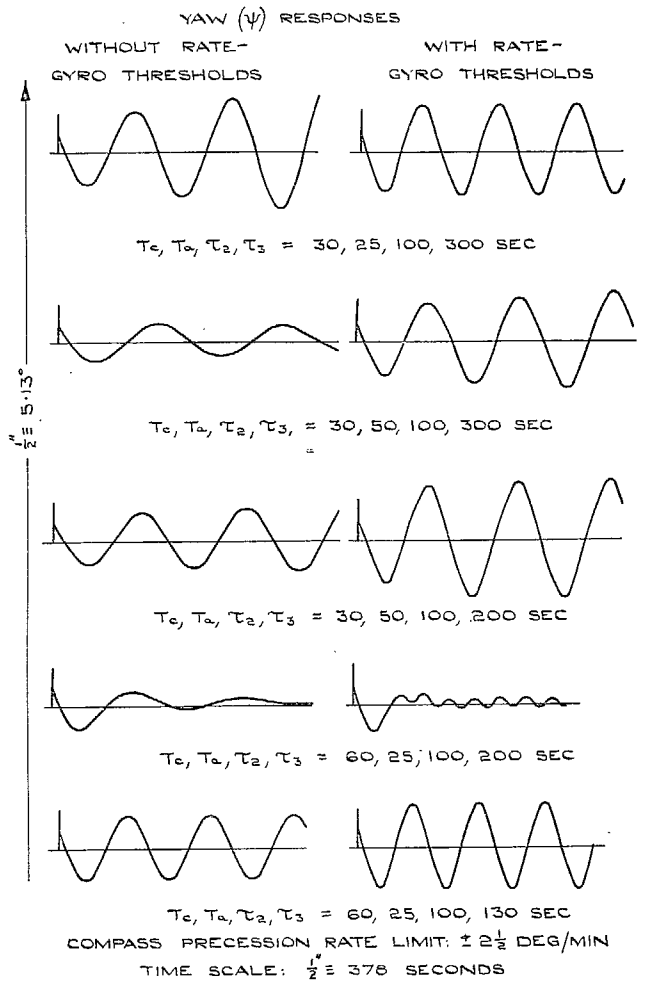

FIG. 26. Sperry stabilizing scheme (Type 1 autopilot).

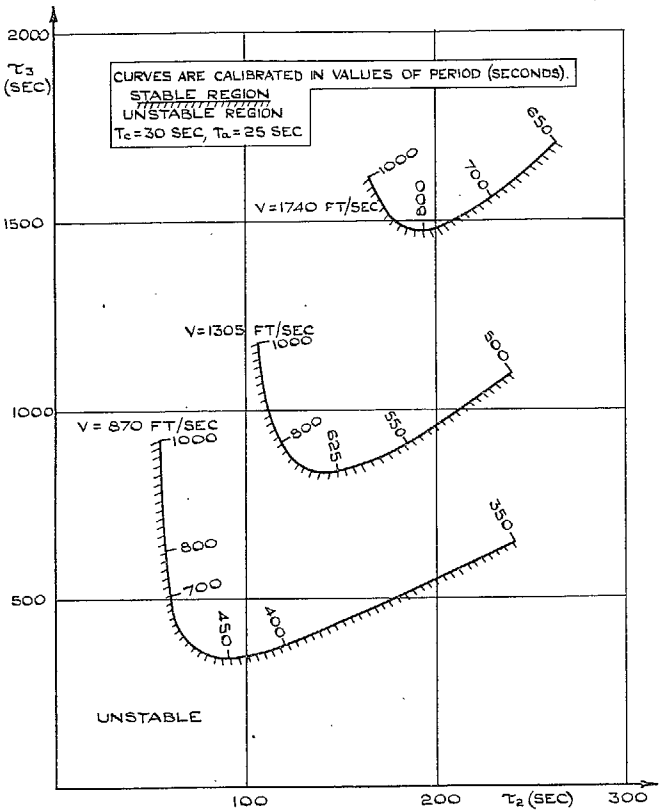

FIG. 27. Effect of changing speed (Sperry scheme, Type 1 autopilot).

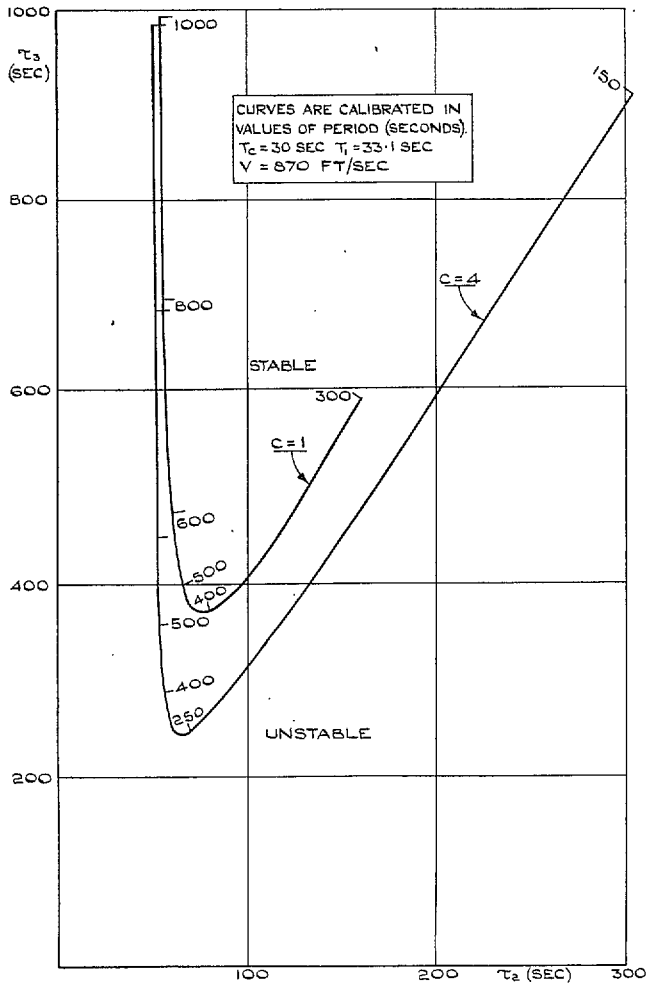

FIG. 28. Sperry stabilizing scheme approximate stability boundaries (Type 2 autopilot).

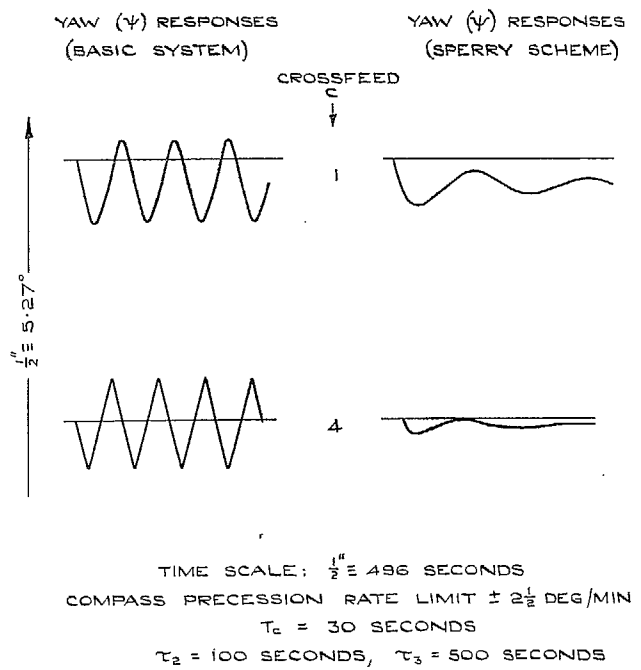

TIME SCALE: 1" ≡ 496 SECONDS
COMPASS PRECESSION RATE LIMIT ± 2½ DEG/MIN
T_c = 30 SECONDS
τ_2 = 100 SECONDS, τ_3 = 500 SECONDS

FIG. 29. Sperry stabilizing scheme (Type 2 autopilot). No erection on vertical gyro.

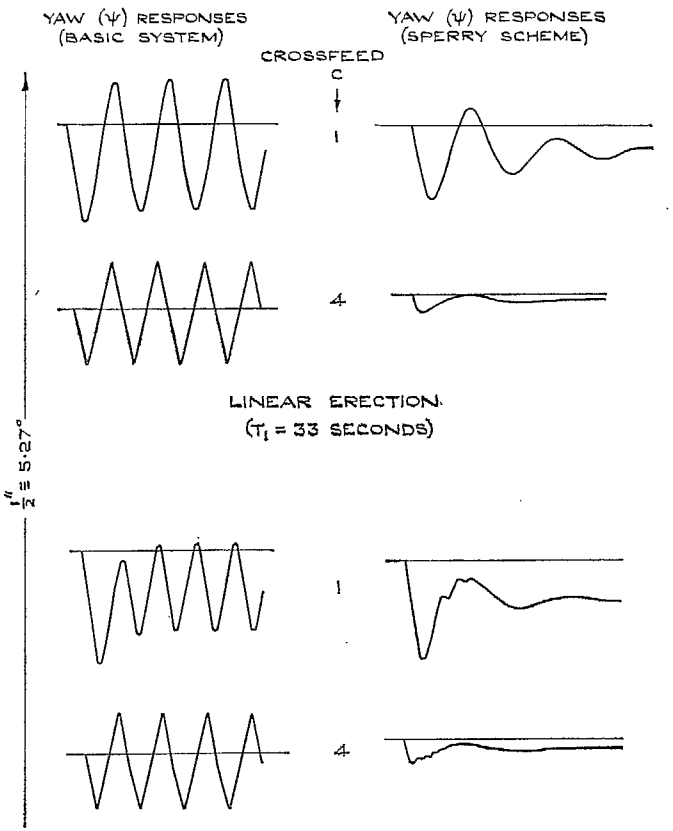

BANG-BANG ERECTION
TIME SCALE: 1" ≡ 496 SECONDS
COMPASS PRECESSION RATE LIMIT ± 2½ DEG/MIN
VERTICAL-GYRO ERECTION RATE LIMIT ± 2½ DEG/MIN
T_c = 30 SECONDS, τ_2 = 100 SECONDS, τ_3 = 500 SECONDS

FIG. 30. Sperry stabilizing scheme (Type 2 autopilot). Linear and bang-bang erection on vertical gyro.

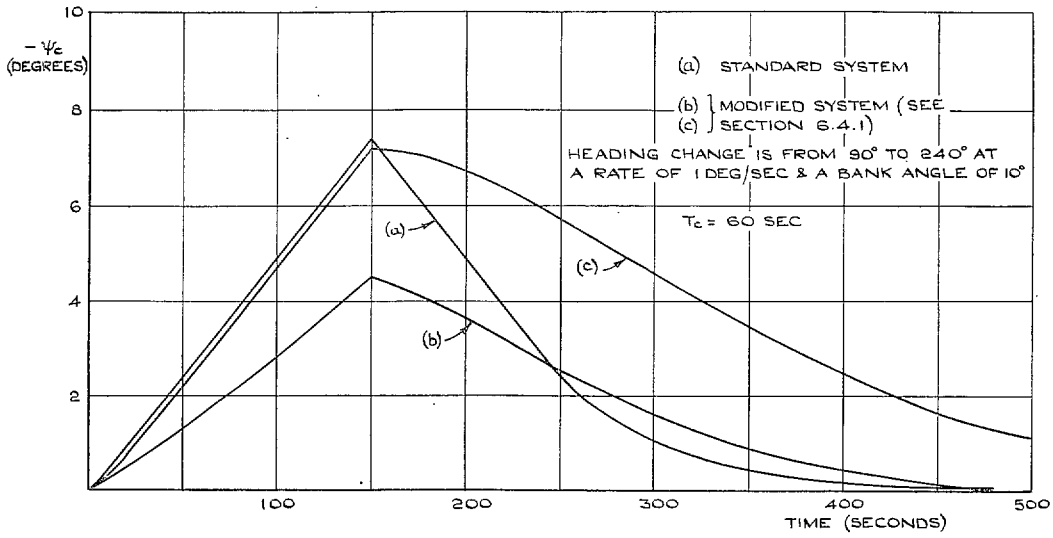

FIG. 31. Turn errors in standard and modified systems.

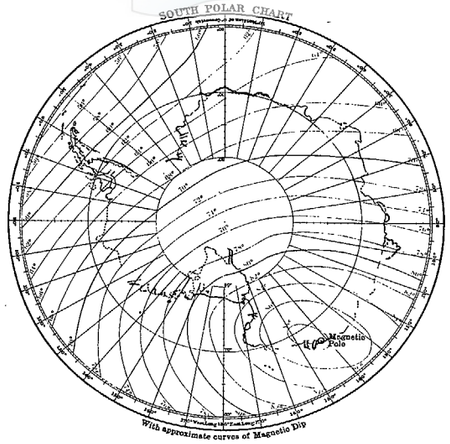

CURVES OF MAGNETIC DIP, 1955.

Reduced to the Epoch 1955·0 from observations by the Officers of Her Majesty's Navy
and from Surveys carried out by Colonial and Foreign Governments and by the Carnegie Institution of Washington.
Compiled at the Royal Greenwich Observatory.
North Pole Dip Red South Pole Dip Blue

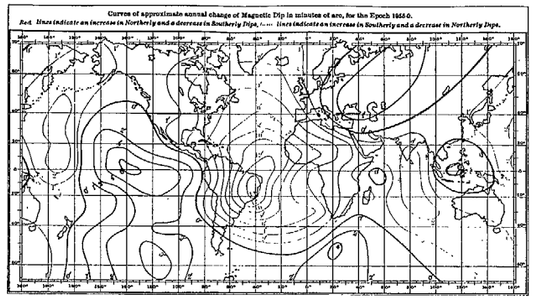

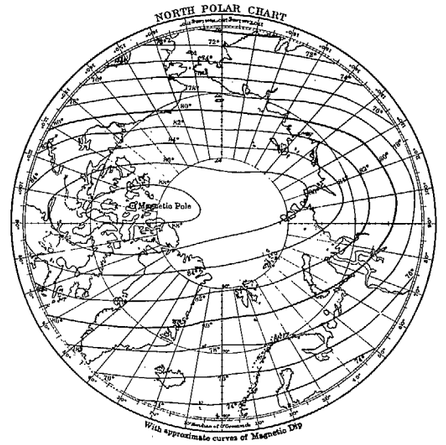

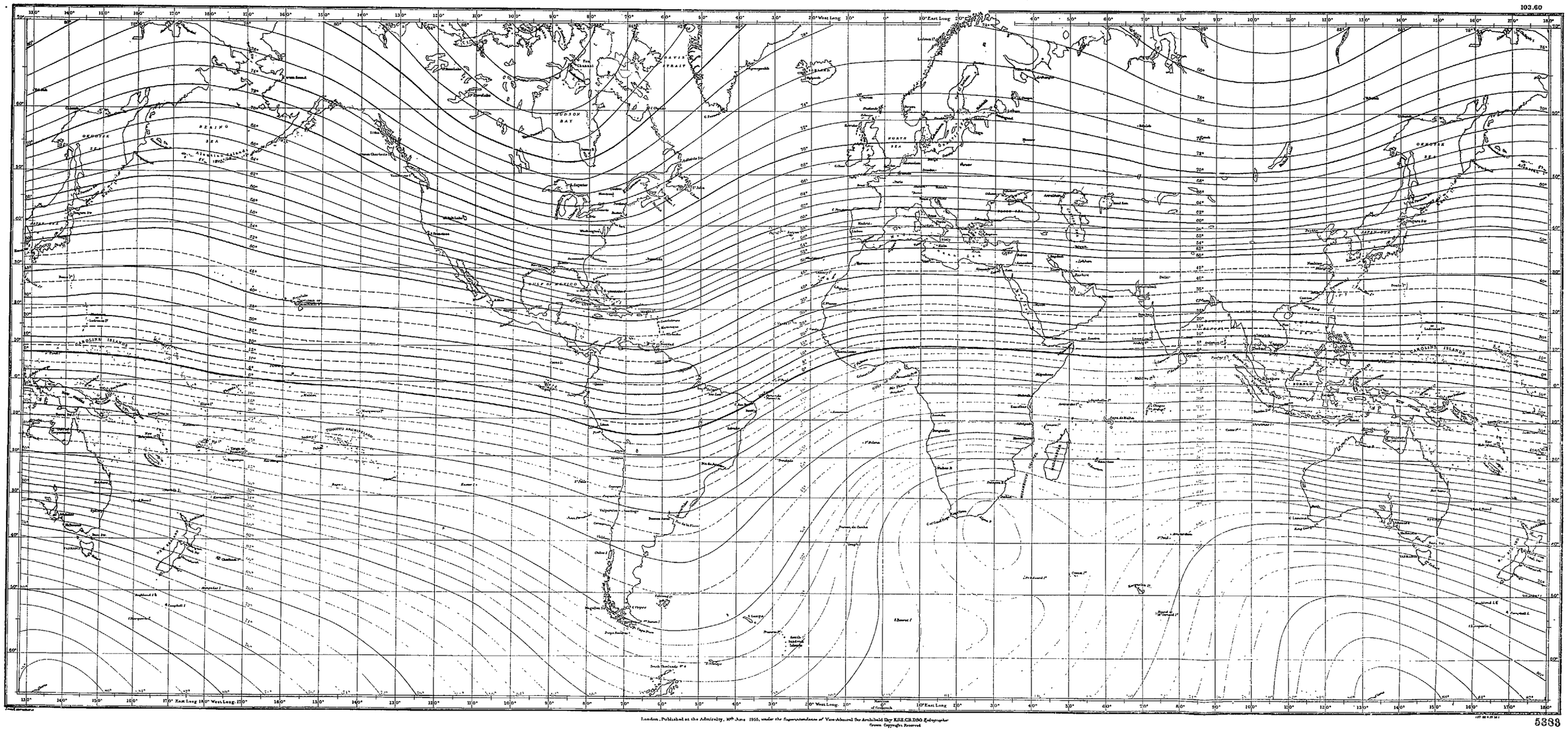

London, Published at the Admiralty, 30th June 1955, under the Superintendence of Vice-Admiral Sir Archibald Day K.B.E. C.B. D.S.O. Hydrographer
Crown Copyright Reserved.

FIG. 32. World chart of curves of magnetic dip.

SOUTH POLAR CHART

CURVES OF HORIZONTAL MAGNETIC INTENSITY, 1955.

Reduced to the Epoch 1955·0 from Observations by the Officers of Her Majesty's Navy
and from Surveys carried out by Colonial and Foreign Governments and by the Carnegie Institution of Washington.

Compiled at the Royal Greenwich Observatory

The Curves are drawn for Values in centimetre-gramme-second units.

Curves of approximate annual change of the Horizontal Intensity in units of the fourth decimal place for the Epoch 1955·0.
Solid lines indicate an increase of the Horizontal Intensity; Pecked lines indicate a decrease of the Horizontal Intensity.

NORTH POLAR CHART

With approximate Curves of Horizontal Magnetic Intensity

London: Published at the Admiralty, 22nd April 1955 *under the Superintendence of Vice-Admiral Sir Archibald Day* K.B.E., F.R.S., F.R.A.S. *Hydrographer*
Crown Copyright Reserved

5379

FIG. 33. World chart of curves of horizontal magnetic intensity.

Publications of the Aeronautical Research Council

ANNUAL TECHNICAL REPORTS OF THE AERONAUTICAL RESEARCH COUNCIL (BOUND VOLUMES)

1942 Vol. I. Aero and Hydrodynamics, Aerofoils, Airscrews, Engines. 75*s.* (post 2*s.* 9*d.*)
Vol. II. Noise, Parachutes, Stability and Control, Structures, Vibration, Wind Tunnels. 47*s.* 6*d.* (post 2*s.* 3*d.*)

1943 Vol. I. Aerodynamics, Aerofoils, Airscrews. 80*s.* (post 2*s.* 6*d.*)
Vol. II. Engines, Flutter, Materials, Parachutes, Performance, Stability and Control, Structures. 90*s.* (post 2*s.* 9*d.*)

1944 Vol. I. Aero and Hydrodynamics, Aerofoils, Aircraft, Airscrews, Controls. 84*s.* (post 3*s.*)
Vol. II. Flutter and Vibration, Materials, Miscellaneous, Navigation, Parachutes, Performance, Plates and Panels, Stability, Structures, Test Equipment, Wind Tunnels. 84*s.* (post 3*s.*)

1945 Vol. I. Aero and Hydrodynamics, Aerofoils. 130*s.* (post 3*s.* 6*d.*)
Vol. II. Aircraft, Airscrews, Controls. 130*s.* (post 3*s.* 6*d.*)
Vol. III. Flutter and Vibration, Instruments, Miscellaneous, Parachutes, Plates and Panels, Propulsion. 130*s.* (post 3*s.* 3*d.*)
Vol. IV. Stability, Structures, Wind Tunnels, Wind Tunnel Technique. 130*s.* (post 3*s.* 3*d.*)

1946 Vol. I. Accidents, Aerodynamics, Aerofoils and Hydrofoils. 168*s.* (post 3*s.* 9*d.*)
Vol. II. Airscrews, Cabin Cooling, Chemical Hazards, Controls, Flames, Flutter, Helicopters, Instruments and Instrumentation, Interference, Jets, Miscellaneous, Parachutes. 168*s.* (post 3*s.* 3*d.*)
Vol. III. Performance, Propulsion, Seaplanes, Stability, Structures, Wind Tunnels. 168*s.* (post 3*s.* 6*d.*)

1947 Vol. I. Aerodynamics, Aerofoils, Aircraft. 168*s.* (post 3*s.* 9*d.*)
Vol. II. Airscrews and Rotors, Controls, Flutter, Materials, Miscellaneous, Parachutes, Propulsion, Seaplanes, Stability, Structures, Take-off and Landing. 168*s.* (post 3*s.* 9*d.*)

1948 Vol. I. Aerodynamics, Aerofoils, Aircraft, Airscrews, Controls, Flutter and Vibration, Helicopters, Instruments, Propulsion, Seaplane, Stability, Structures, Wind Tunnels. 130*s.* (post 3*s.* 3*d.*)
Vol. II. Aerodynamics, Aerofoils, Aircraft, Airscrews, Controls, Flutter and Vibration, Helicopters, Instruments, Propulsion, Seaplane, Stability, Structures, Wind Tunnels. 110*s.* (post 3*s.* 3*d.*)

Special Volumes

Vol. I. Aero and Hydrodynamics, Aerofoils, Controls, Flutter, Kites, Parachutes, Performance, Propulsion, Stability. 126*s.* (post 3*s.*)
Vol. II. Aero and Hydrodynamics, Aerofoils, Airscrews, Controls, Flutter, Materials, Miscellaneous, Parachutes, Propulsion, Stability, Structures. 147*s.* (post 3*s.*)
Vol. III. Aero and Hydrodynamics, Aerofoils, Airscrews, Controls, Flutter, Kites, Miscellaneous, Parachutes, Propulsion, Seaplanes, Stability, Structures, Test Equipment. 189*s.* (post 3*s.* 9*d.*)

Reviews of the Aeronautical Research Council

1939–48 3*s.* (post 6*d.*) 1949–54 5*s.* (post 5*d.*)

Index to all Reports and Memoranda published in the Annual Technical Reports

1909–1947 R. & M. 2600 (out of print)

Indexes to the Reports and Memoranda of the Aeronautical Research Council

Between Nos. 2351–2449	R. & M. No. 2450	2*s.* (post 3*d.*)
Between Nos. 2451–2549	R. & M. No. 2550	2*s.* 6*d.* (post 3*d.*)
Between Nos. 2551–2649	R. & M. No. 2650	2*s.* 6*d.* (post 3*d.*)
Between Nos. 2651–2749	R. & M. No. 2750	2*s.* 6*d.* (post 3*d.*)
Between Nos. 2751–2849	R. & M. No. 2850	2*s.* 6*d.* (post 3*d.*)
Between Nos. 2851–2949	R. & M. No. 2950	3*s.* (post 3*d.*)
Between Nos. 2951–3049	R. & M. No. 3050	3*s.* 6*d.* (post 3*d.*)
Between Nos. 3051–3149	R. & M. No. 3150	3*s.* 6*d.* (post 3*d.*)

HER MAJESTY'S STATIONERY OFFICE

from the addresses overleaf

Printed and published by
HER MAJESTY'S STATIONERY OFFICE

To be purchased from
York House, Kingsway, London W.C.2
423 Oxford Street, London W.1
13A Castle Street, Edinburgh 2
109 St. Mary Street, Cardiff
39 King Street, Manchester 2
50 Fairfax Street, Bristol 1
35 Smallbrook, Ringway, Birmingham 5
80 Chichester Street, Belfast 1
or through any bookseller

Printed in England

S.O. Code No. 23-3356